Active galactic nuclei (AGNs): a brief observational tour

Yongquan Xue (薛永泉)

Department of Astronomy
University of Science and Technology of China
http://staff.ustc.edu.cn/~xuey

Summary of lectures

- Early history, AGN ABCs, finding AGNs, AGN terminology and unification
- Dissecting AGNs (I): black hole, accretion disk, broad line region
- Dissecting AGNs (II): torus, narrow line region, stars and starburst regions, jets
- Focused lecture: Lifting the veil of deeply buried supermassive black holes in the Universe

Summary of lectures

- Early history, AGN ABCs, finding AGNs, AGN terminology and unification
- Dissecting AGNs (I): black hole, accretion disk, broad line region
- **Dissecting AGNs (II): torus, narrow line region, stars and starburst regions, jets**
- Focused lecture: Lifting the veil of deeply buried supermassive black holes in the Universe

Torus

The central torus

The Torus and AGN Unification

Type I vs. II optical spectral differences have come to be understood as (often) due to orientation-dependent central obscuration by a so-called "torus".

The torus is presumed to be an axisymmetric structure of large height so that, at least at low luminosities, the majority of AGNs are obscured by it.

It is made of a combination of dusty atomic and molecular gas.

The dust causes large extinction in the optical/UV and sometimes even in the NIR.

The Torus and AGN Unification

The torus lies between the BLR and the NLR.

Type 2 AGNs are those obscured by the torus, and emission on the scale of the BLR and smaller is obscured by it.

Models explaining differences between Type 1 and Type 2 AGNs this way are referred to as "unification models".

These models have had much success, though they are not complete and there are likely exceptions.

There appear to be substantial object-to-object variations in the covering factor and geometry of the torus.

Polarization by Scattering and the Unified Model

The early history of the unified model is complex, and several researchers put forward early ideas along these lines.

However, a significant breakthrough came from sensitive studies of the polarization properties of AGNs.

These found "hidden" BLRs in the polarized light from many Type 2 AGNs.

A "mirror" made of electrons or dust is able to scatter some of the small-scale emission around the torus, providing a "periscopic" view of the inner regions.

This scattering polarizes the relevant radiation.

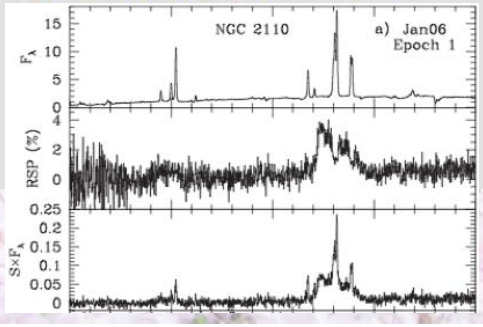

X-rays and the Unified Model

Additional evidence for the unified model comes from studies of X-ray absorption and iron K line emission in Type 2 AGNs.

The X-ray opacity of gas is strongly energy dependent, and high-energy X-rays can in many cases pierce through the torus.

This enables the column density through the torus to be estimated, with values of 10^{22}-10^{24} cm^{-2} often being found.

Some Type 2 AGNs have very large column densities that cannot be pierced even with high-energy X-rays – these are called "Compton-thick" AGNs.

Additional evidence for the unified model comes from the very high EWs of iron K line emission in some Type 2 AGNs. The large EW arises when the direct continuum is blocked but the torus and/or mirror are able to produce iron K lines.

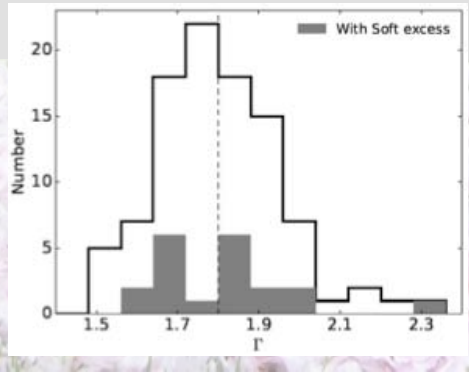

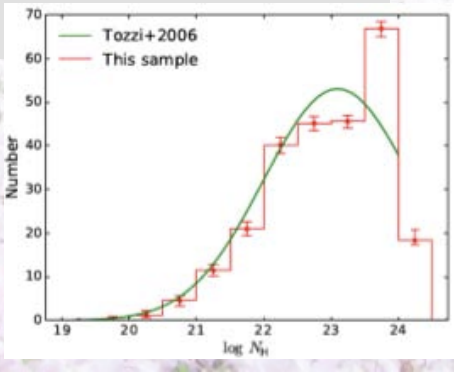

Piercing the Torus with High-Energy X-rays

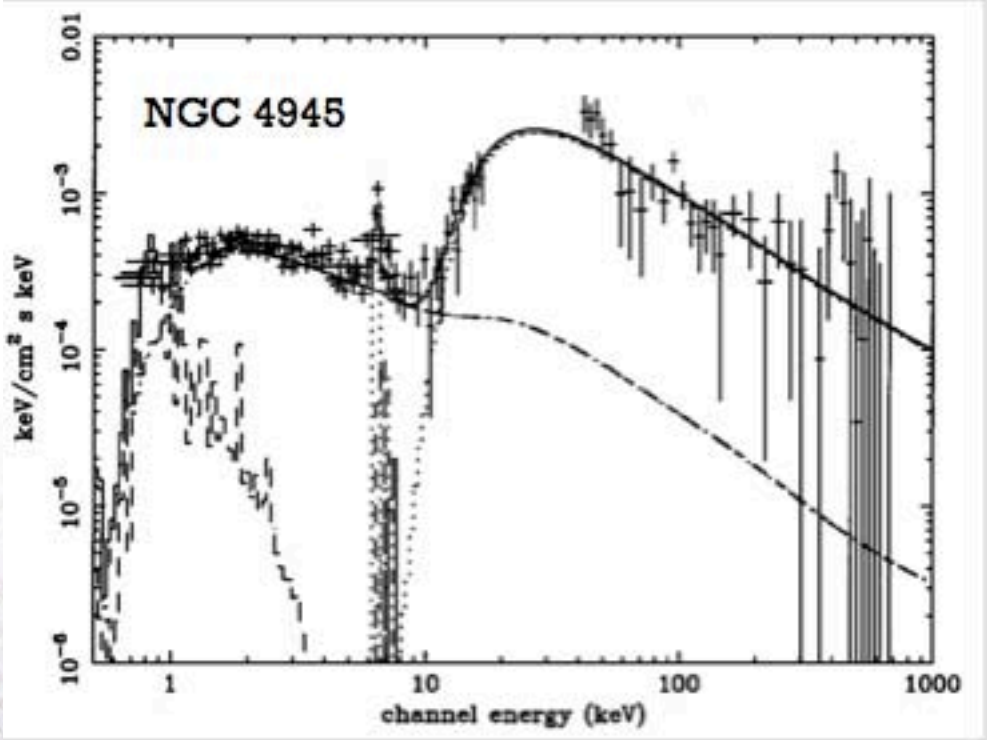

Done et al. (1996)

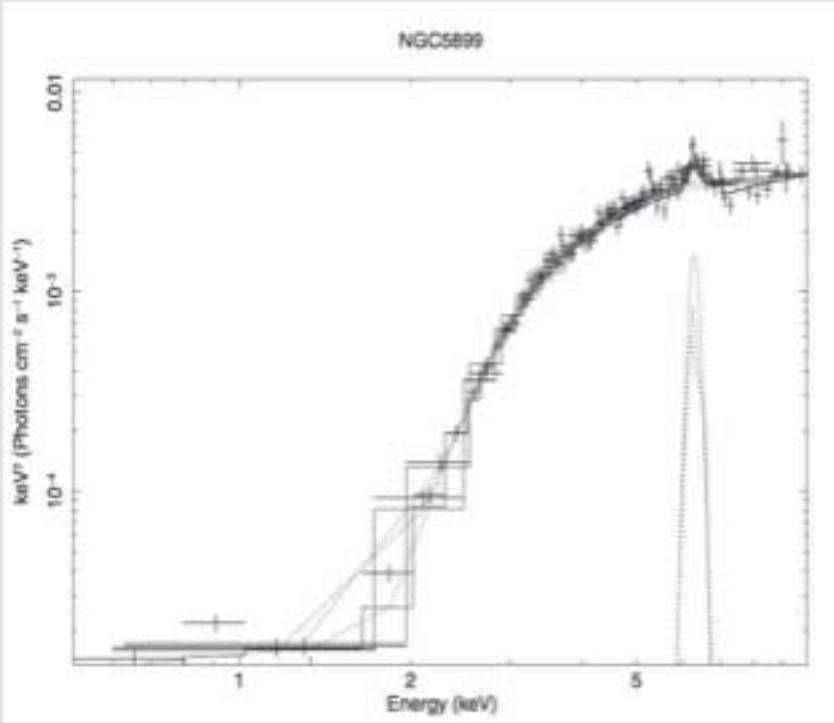

Vasudevan et al. (2013)

How Big is the Torus?

We know the torus must lie between the BLR and NLR, but we can be more specific.

We can now directly measure the size of the torus using

- Dust reverberation mapping between the *V*-band and *K*-band light curves.
- Interferometry in the NIR and MIR.

The size of the torus appears to scale as $L^{0.5}$.

The inner edge of the torus is at about 3 times the BLR radius for Hβ as determined from reverberation mapping.

Direct Measurements of the Torus Size

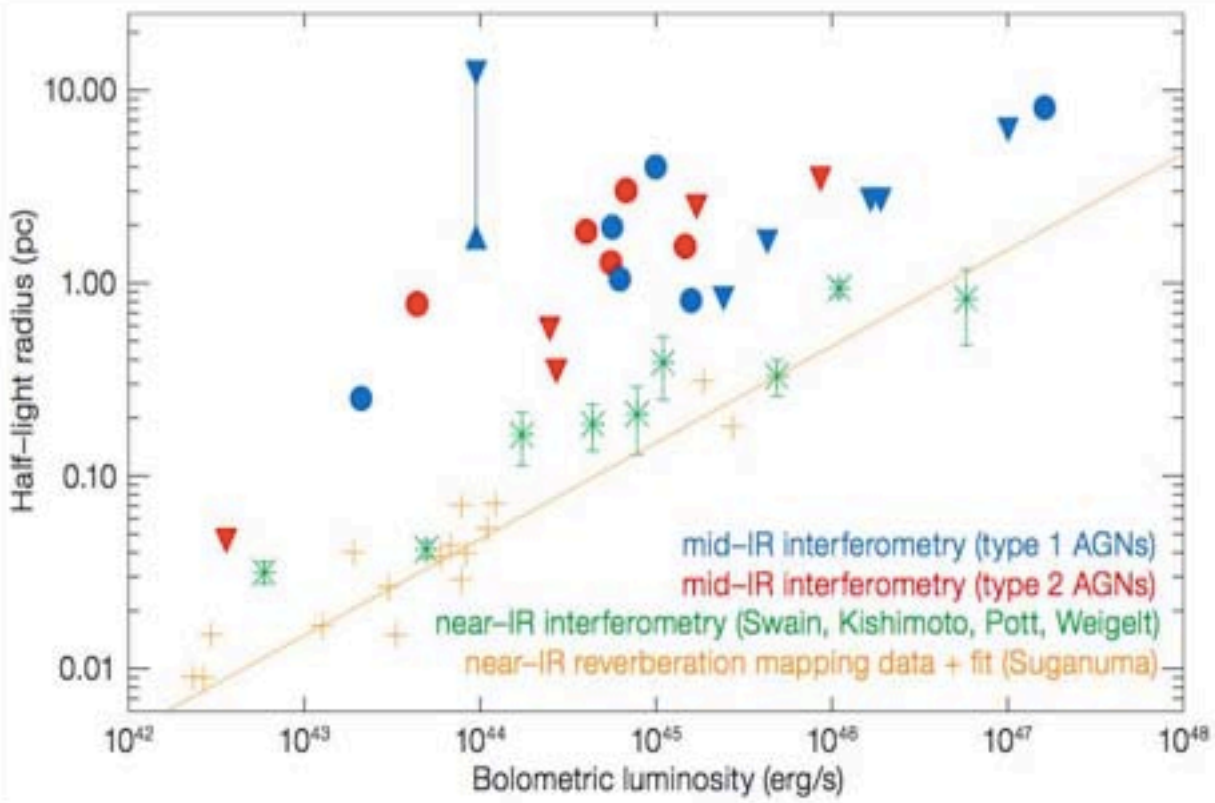

Figure 5. Size–luminosity relation for AGNs probing different regions of the torus: blue/ red points are MIDI measurements from the MIDI AGN Large Programme + archive for type 1/type 2 sources (statistical errors are smaller than symbol sizes); green crosses are NIR interferometry with both the Keck-Interferometer and AMBER/VLTI; orange pluses are from NIR dust reverberation mapping. Filled triangles show limits. Taking both the limits and the determined half-light radii into account shows that the mid-infrared size is less strictly correlated with luminosity than the innermost radius of dust that is seen in the NIR.

torus ~0.01-10 pc; beyond dust sublimation radius;
likely to contain dust and molecular gas

Burtscher et al. (2013)

NIR / MIR Torus Spectra

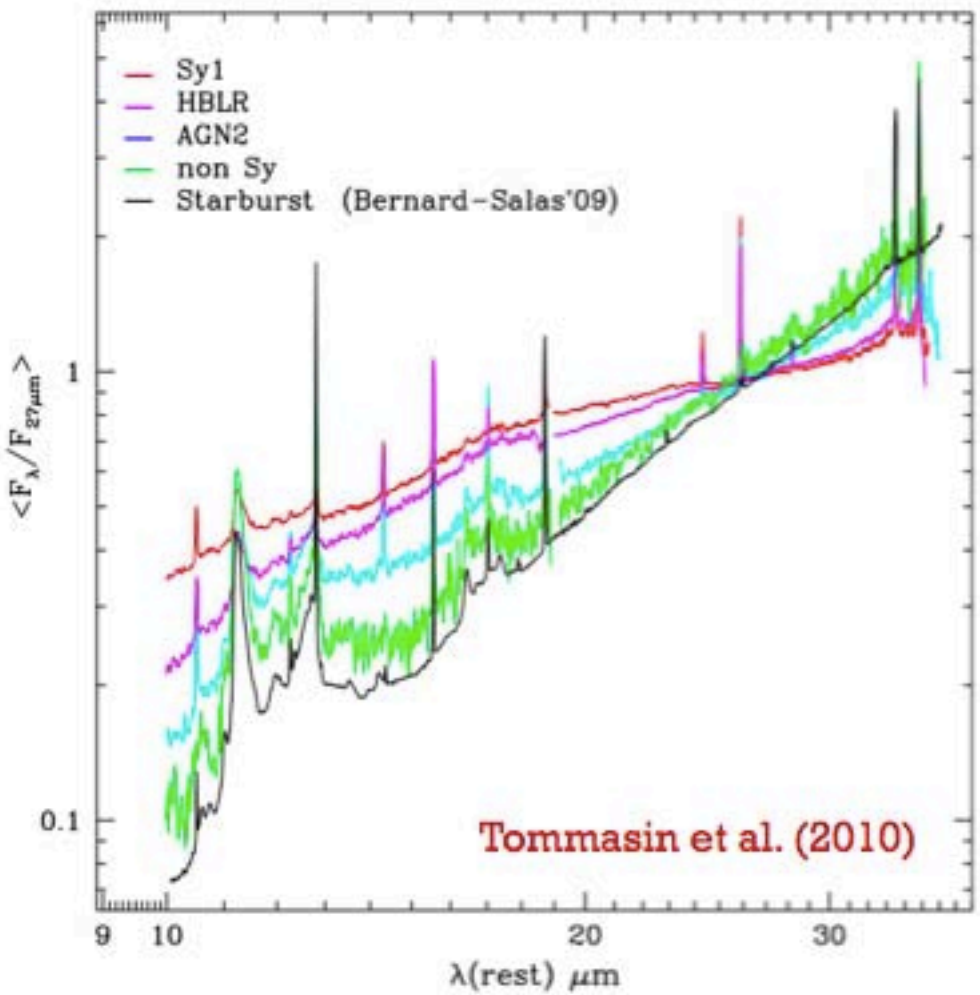

Figure 14. Average high-resolution spectra for our classes of galaxies, compared with the mean high-resolution spectrum of starburst galaxies.

NIR / MIR spectroscopy of dust emission places further constraints upon the torus properties.

If the torus were continuous over the range of radii observed, one would expect substantially hotter dust emission in Type 1 AGNs than Type 2 AGNs.

In Type 1 AGNs one could see the hot inner wall of the torus, while in Type 2 AGNs one could only see cooler dust at large radii.

But this is not observed. This result and others have led to a preference for "clumpy" torus models.

A Clumpy Torus

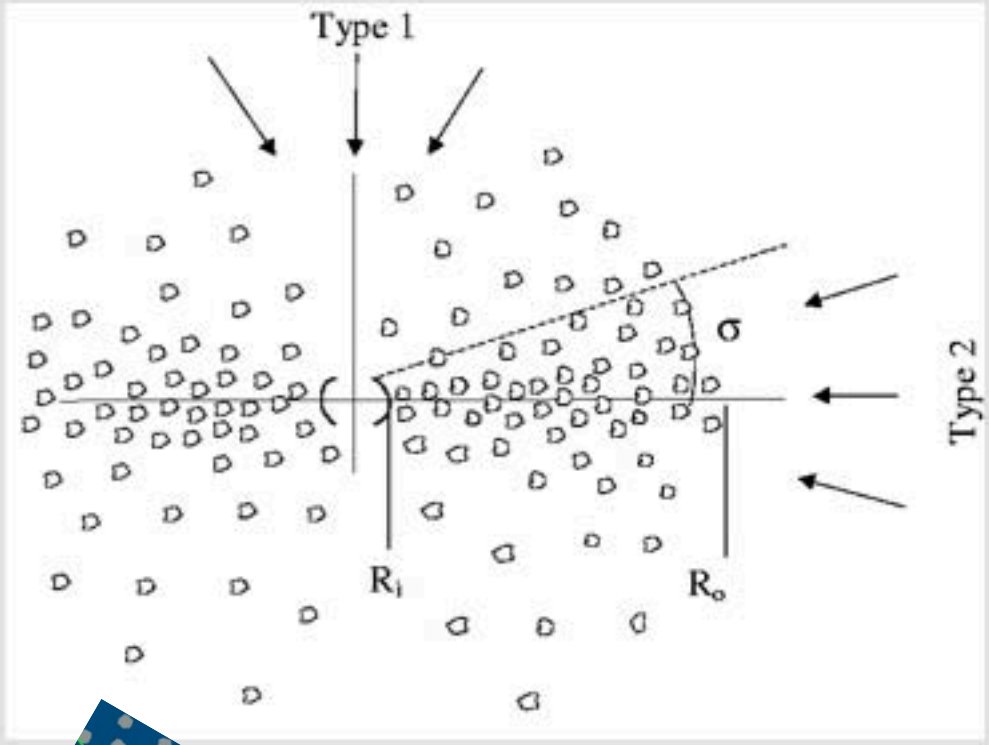

Nenkova et al. (2002, 2006)

Clumpy torus models break the strict correlation between dust temperature and distance, allowing clumps further out to be heated by the central radiation.

They improve agreement with the data.

AGN type would then be an orientation-dependent probability.

To explain the full NIR / MIR spectrum, one must also include NLR dust emission and a detailed treatment of the hot (1500-2000 K) graphite dust at the inner wall of the torus.

VS.

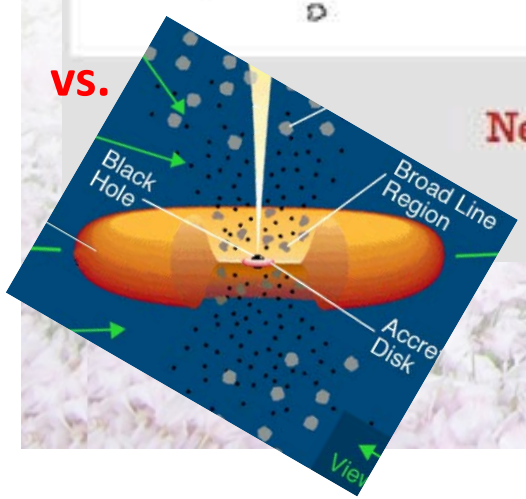

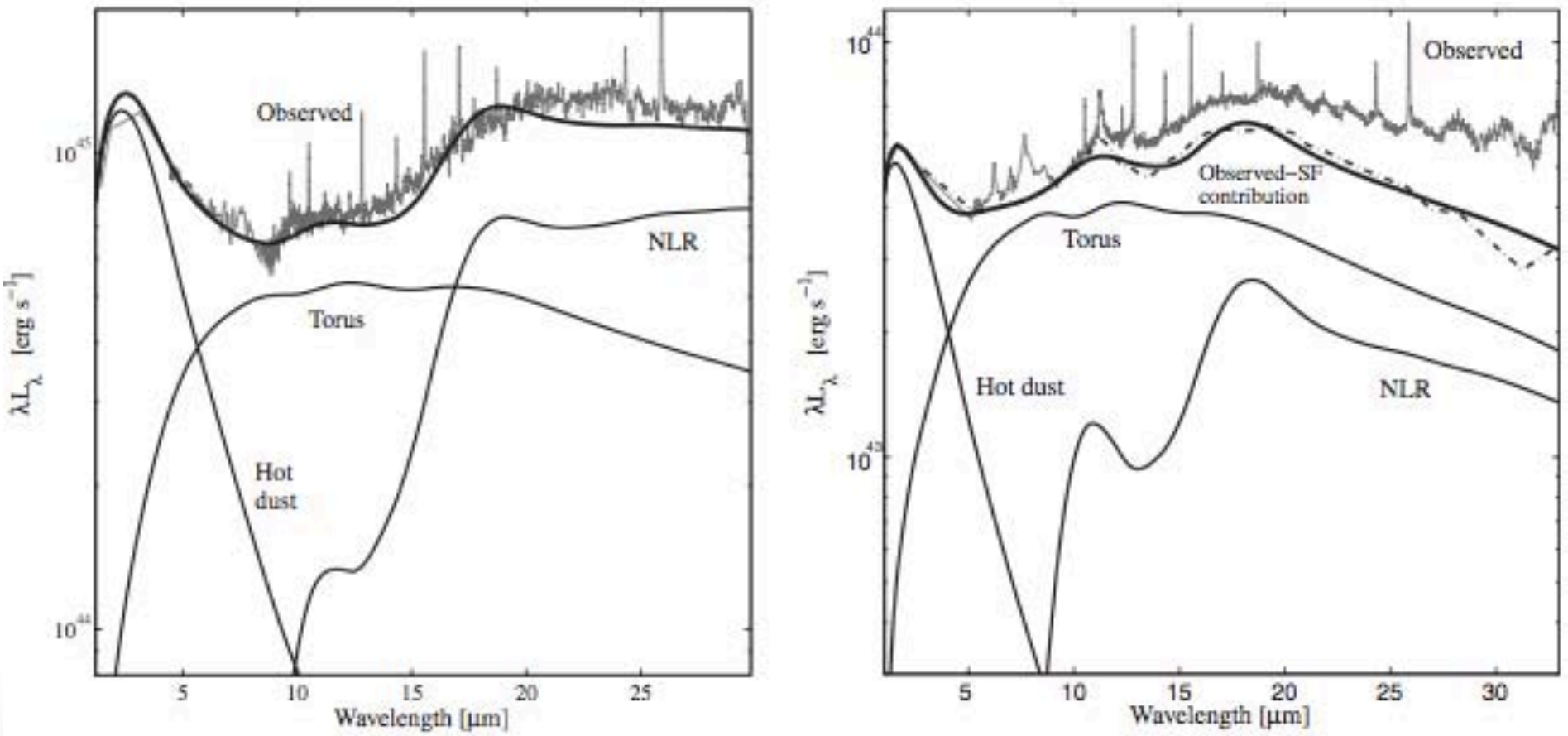

Figure 7.35. Three-component model fits to the spectra of Mrk 705 and PG 2349, both luminous type-I AGNs. The models includes hot (pure graphite) dust, clumpy torus, and NLR dust, as marked. A SF contribution was subtracted from the observed spectra prior to the fits. This contribution is much larger in the case of Mrk 705 (adapted from Mor and Netzer, 2012).

works at some parts of the spectra but not all; improvements needed

Some Characteristic Torus Properties

Keplerian velocities at the torus distance are ~ 1000 km s^{-1}.

Density of torus "clumps" are ~ 10^5-10^7 cm^{-3}.

The estimated mass of the torus is only a small fraction of the SMBH mass.

The Nature of the "Torus"

The torus is likely a dynamic system, being part of the general flow of matter from the galaxy's center to the SMBH.
(changing-look AGNs)

This can help explain its large *H/R*, resolving stability issues.

But the details remain unclear.

One attractive idea is that the torus is part of an outer disk wind where dust is able to form – large disk required.

Another idea is that the torus may actually a warped outer accretion disk – large disk required.

The Torus as a Disk Wind

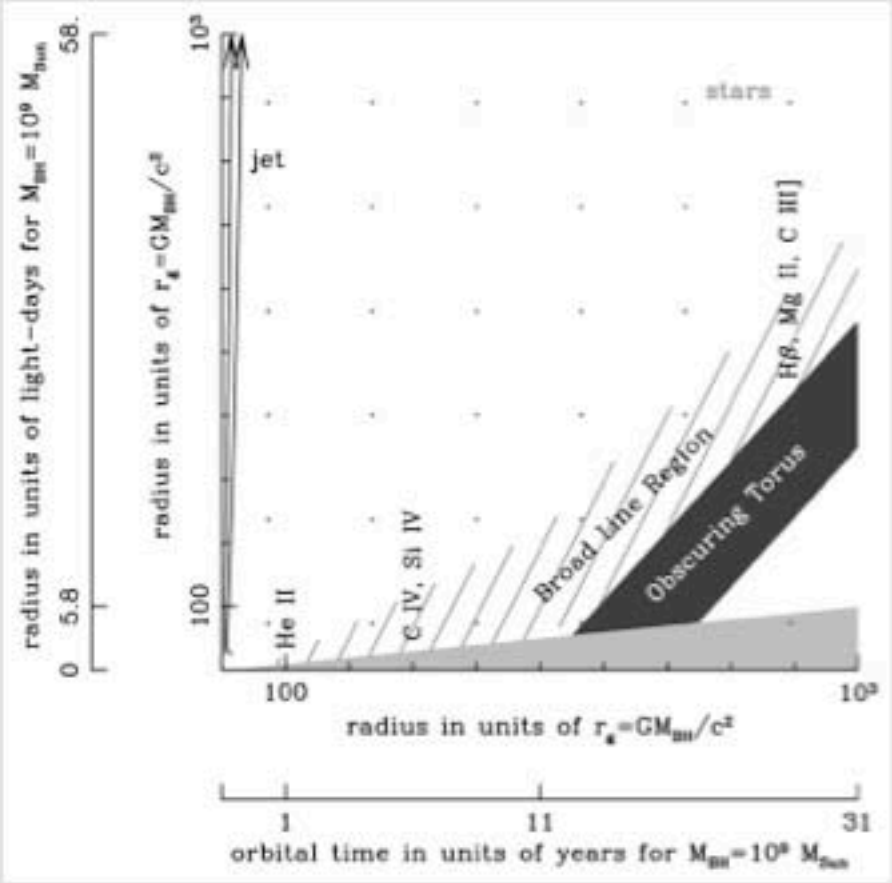

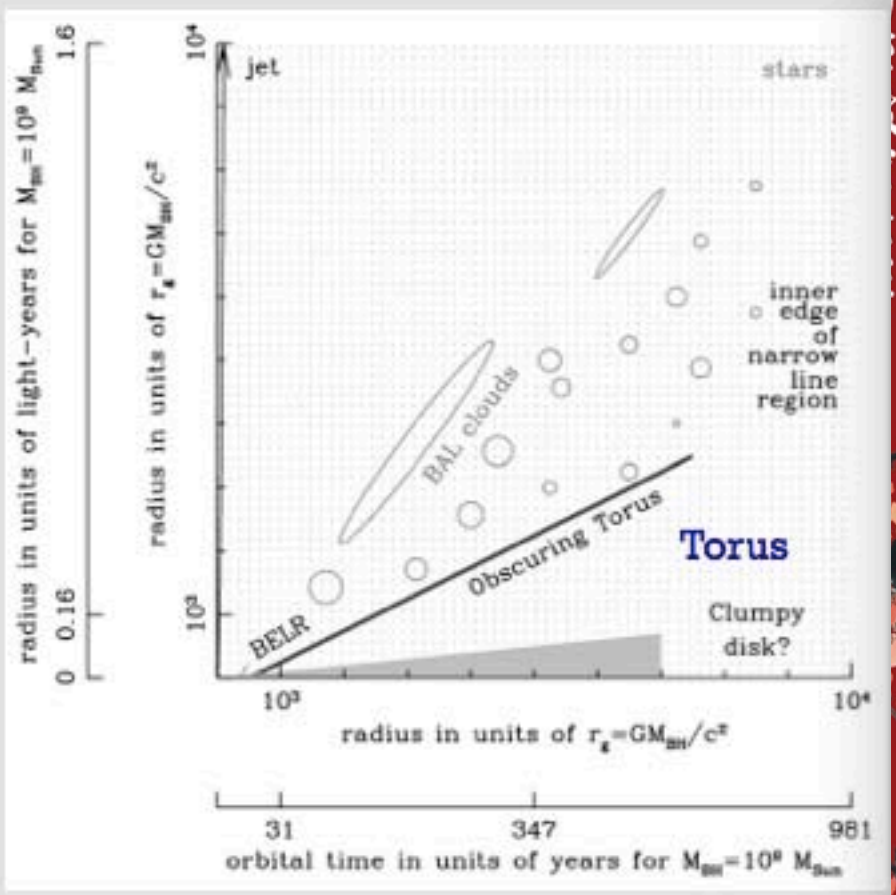

Courtesy of Pat Hall

Narrow line region

BLR vs. NLR

Lines are Kinematically Composite

Broad components column ~1e23 cm^{-2}; T~1e4 K; C_f~0.1

- Doppler widths of 1000-25000 km s^{-1}.
- Arise in gas with density n_e ~10^9-10^{11} cm^{-3} (as determined from strengths of certain density sensitive lines like [O III] and CIII]). largely dust free
- From the "Broad Line Region".

Narrow components column ~1e20-1e21 cm^{-2}; T~1e4-2.5e4 K; C_f~a few %

- Doppler widths typically less than 900 km s^{-1}.
- Arise in relatively low-density gas (n_e ~ 10^3 cm^{-3}).
- From the "Narrow Line Region". likely contain dust

similar ionization parameter to that in BLR (both with $U_{hydrogen}$~0.01)

Basic Points about the NLR

Largest spatial scale where ionizing radiation from the AGN dominates.

(beyond NLR, stellar ionization dominates)

NLR can be spatially resolved in the optical; has sizes of ~ 100+ pc in local Seyferts (and even larger in quasars).

Can map out physical and kinematic properties directly to some extent.

Imaging the NLR with HST

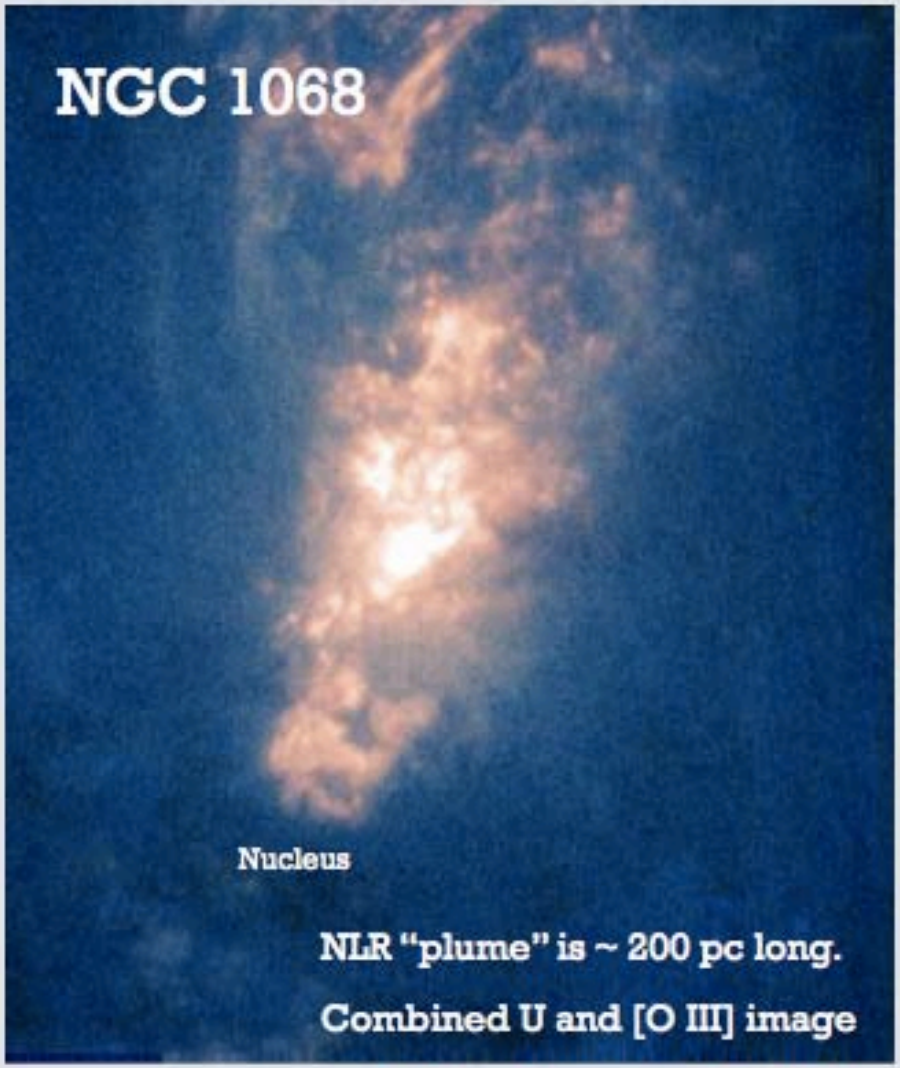

Macchetto et al. (1994)

The line emission region is clumpy and complex.

NLR is clearly not spherically symmetric, but rather is roughly axisymmetric.

NLR axis generally coincides with radio axis in cases where extended linear radio emission is detected.

In some sources, we see strong line emission from regions where the radio jet is colliding with the ISM and causing shocks – an additional source of ionization.

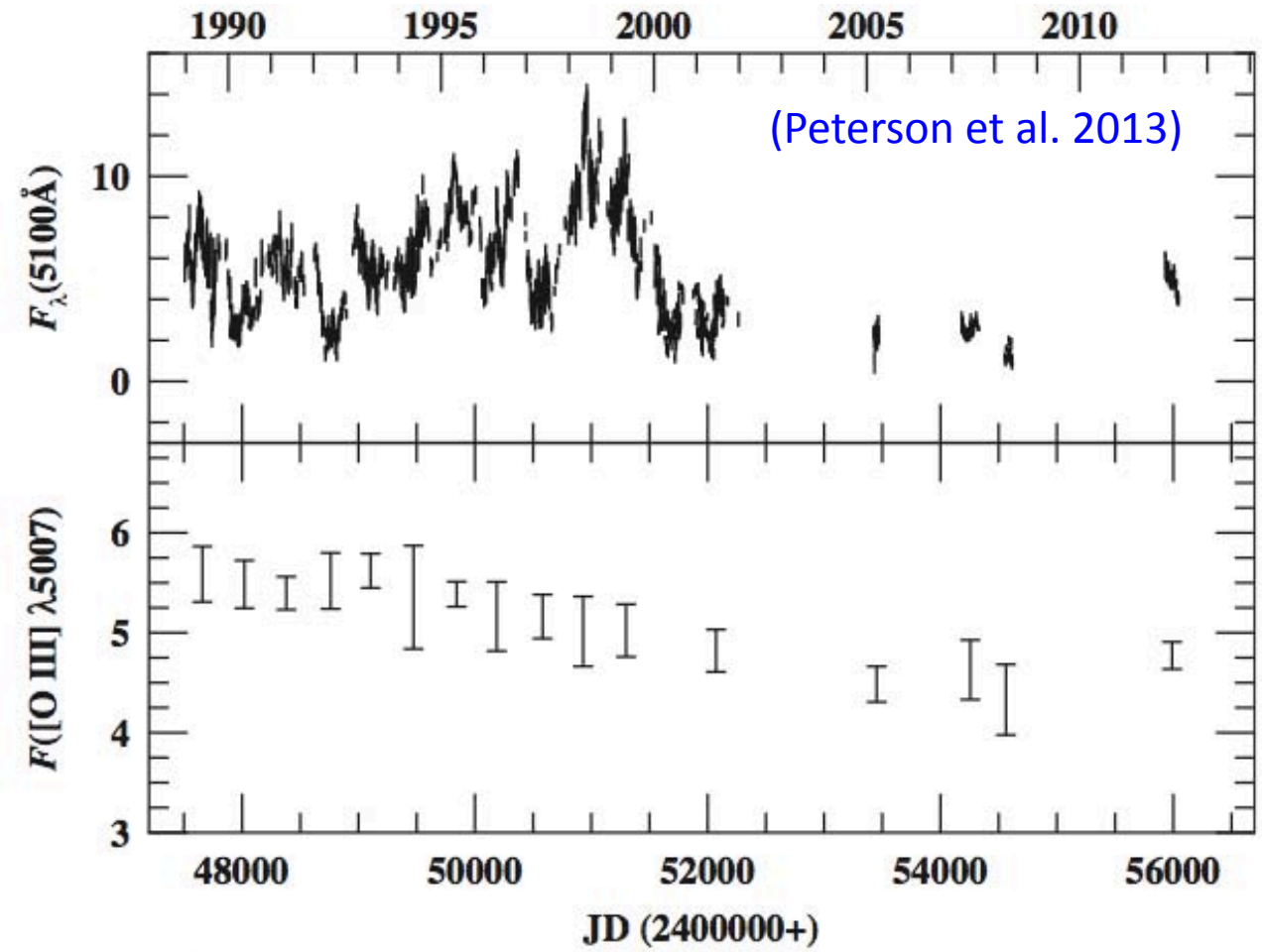

Figure 1. Top panel: observed-frame 5100 Å AGN continuum flux as a function of time, calibrated to a constant value of the [O III] λ5007 flux with a host-galaxy contribution (Table 4) removed, in units of 10^{-15} erg s^{-1} cm^{-2} Å^{-1}. Original sources of data are cited in the notes to Table 3. Bottom panel: observed-frame time-averaged [O III] λ5007 fluxes measured from spectra taken on nights that observers recorded night-sky conditions to be "clear" or "photometric," in units of 10^{-13} erg s^{-1} cm^{-2}, as given in Table 3.

- NLR size of the well-studied Seyfert 1 galaxy NGC 5548:

- narrow [OIII] 4959, 5007 emission-line variability obs.: slow and small variability, ~20 years of monitoring

- NLR has a radius of only 1-3 pc and is denser (n_e~1e5 cm^{-3}) than previously supposed

- surprising results: compact NLR!

NLR: Basic Properties

FWHM values are 200-900 km s^{-1}, with line profiles varying across NLR.

See a wide range of ionization states:

- Low ionization (e.g., [O I] λ6300)
- High ionization (e.g., [O III] λλ4959, 5007)
- Sometimes even very highly ionized species (e.g., iron coronal lines)

From line ratios, infer that the NLR is mostly photoionized by the AGN continuum (with some likely additional ionization by shocks from radio jets).

NLR: Basic Properties

Density is sufficiently low to allow forbidden transitions. Varies from 10^2-10^5 cm^{-3} across the NLR.

From line ratios, infer temperatures of ~ 10000-25000 K, again varying across the NLR.

dust can survive in the NLR and cause self-extinction. Can largely overcome using near-infrared lines.

Estimated total mass of the NLR in Seyferts is ~ 10^6 solar masses.

Emission-line strengths often comparable to those from BLR since emissivity (~ n_e^2) is much lower.

NLR Luminosity Dependence

NLR line EWs drop with increasing continuum luminosity, and are often undetectable in high-luminosity quasars.

NLR becoming larger than the host galaxy? (ENLRs)

$$\log \frac{R_{\rm NLR}}{\rm pc} = 0.52 \log L_{[\rm OIII]} - 18.5$$

ENLRs are clearly seen in a number of high-L AGNs.

The formula cannot hold for all AGNs, e.g.:
Very high-L AGNs may not contain an NLR, with the observed EW([OIII]) being very small and absence of [OIII] lines in some cases. (if L_{bol}~1e48 erg/s, then NLR size >~50 kpc, far beyond host-galaxy size, thus running out of gas?)

R~L^0.5 for BLR, torus, and NLR!

Why is the NLR Important?

Line peaks provide useful systemic redshifts for AGNs.

Useful spectral calibrator since NLR lines should not vary.

Useful as a bolometer for inferring AGN total power.

Dynamics tells us about AGN fueling and/or outflows.

Anisotropic illumination provides clues about AGN geometry and orientation.

The NLR as a Bolometer

NLR lines can be used to estimate rough bolometric luminosities, even for obscured AGNs.

Emitted from a region larger than any nuclear obscuration.

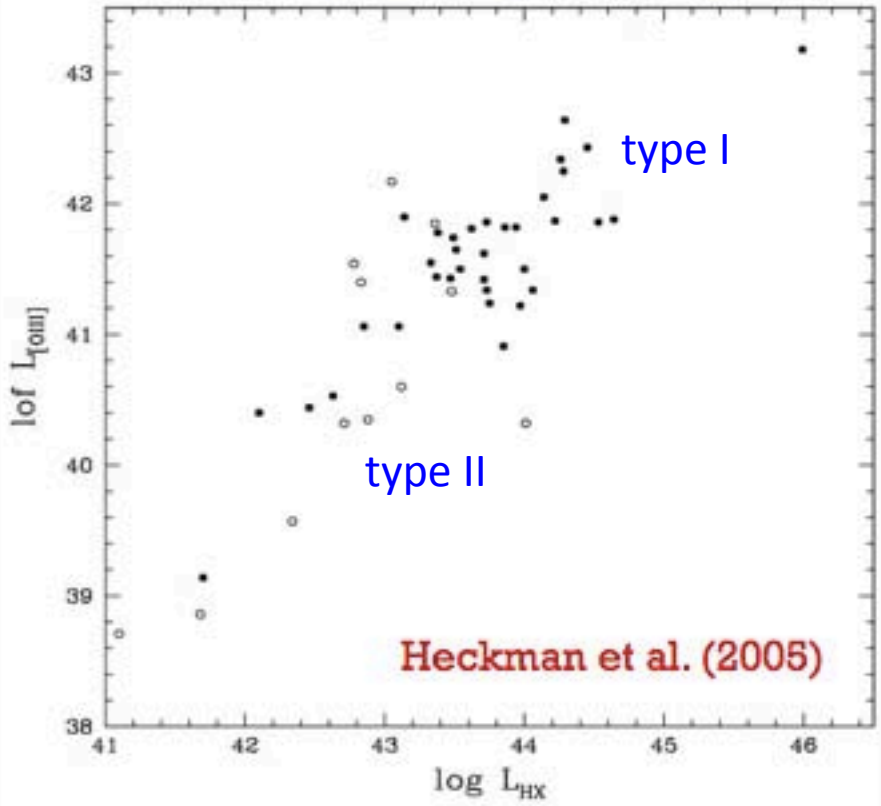

FIG. 2.—Plot of the hard X-ray (3–20 keV) vs. the [O III] λ5007 luminosities for the AGNs in Fig. 1. The Type 1 AGNs are plotted as filled circles and the Type 2 AGNs as hollow circles. Luminosities are in units of ergs s^{-1}.

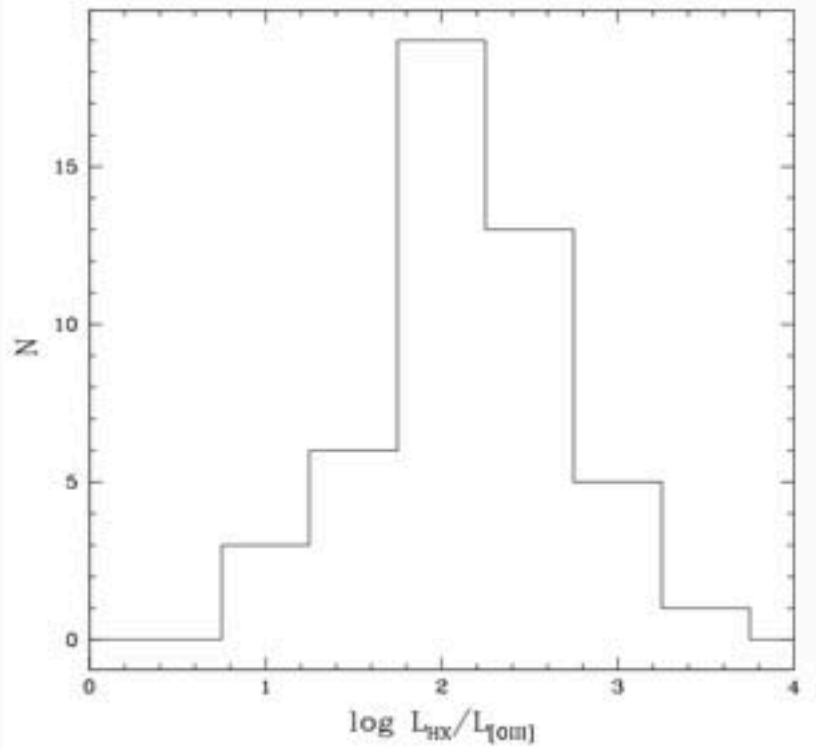

FIG. 1.—Histogram of the log of the ratio of the hard X-ray (3–20 keV) to [O III] λ5007 luminosities for a sample of 47 local AGNs selected on the basis of their hard X-ray flux (the SR04 sample). The distribution has a mean of 2.15 dex and a standard deviation of 0.51 dex. There is no significant difference between the Type 1 and 2 AGNs in this sample (see text for details).

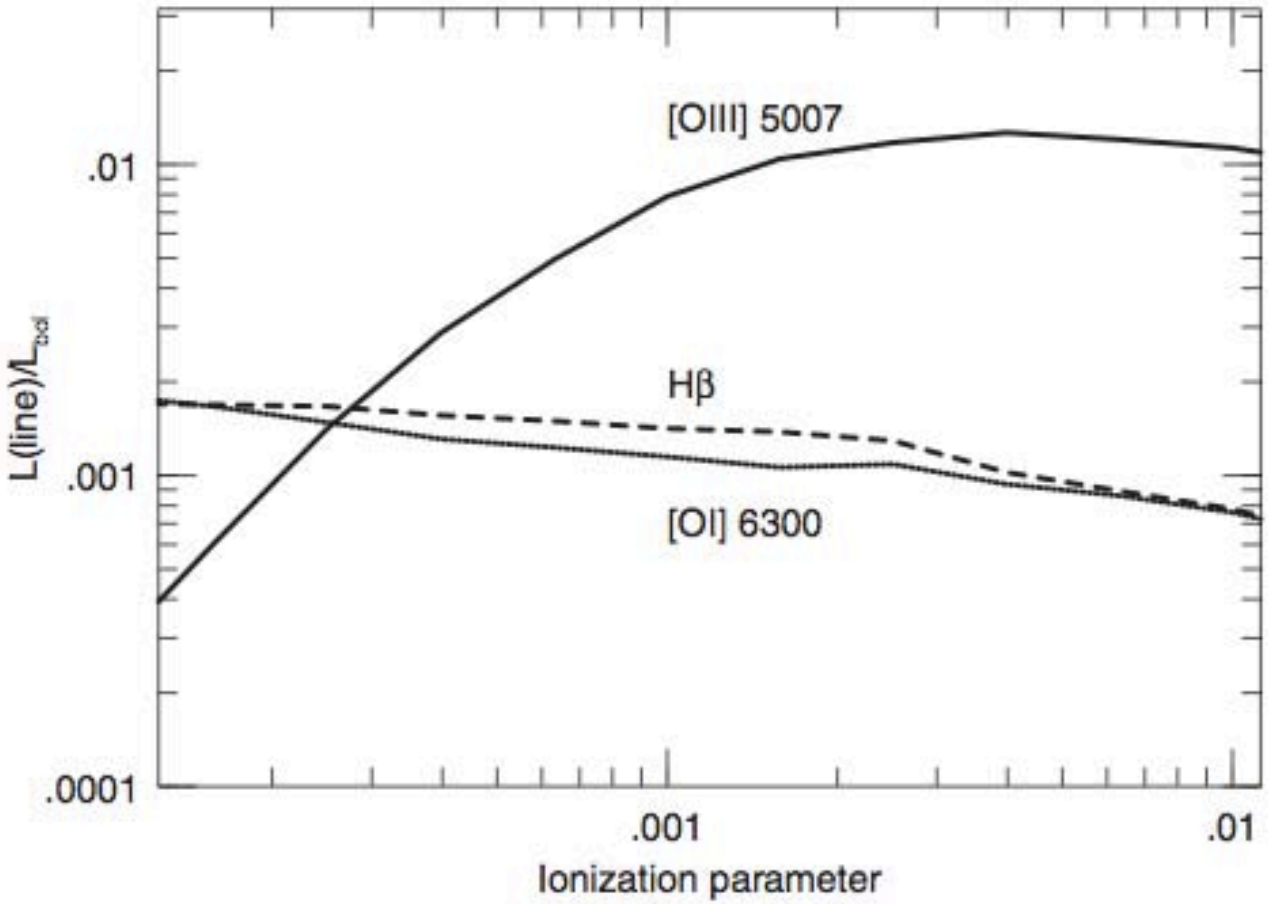

Figure 7.25. Relative line-to-continuum luminosities for strong narrow emission lines. The NLR is assumed to be made of constant-pressure dusty clouds with solar composition, $N_e = 10^3$ cm^{-3}, and full covering of the central source. The SED of the central source is characterized by $\alpha_{ox} = 1.05$ typical of low-luminosity AGNs. The [O III] λ5007 luminosity is a strong function of the ionization parameter, but the other two lines have much weaker dependences (adapted from Netzer, 2009).

$$\log L_{\rm bol} \simeq 3.8 + 0.25 \log L([{\rm O\,III}]\,\lambda 5007) + 0.75 \log L([{\rm O\,I}]\,\lambda 6300)$$

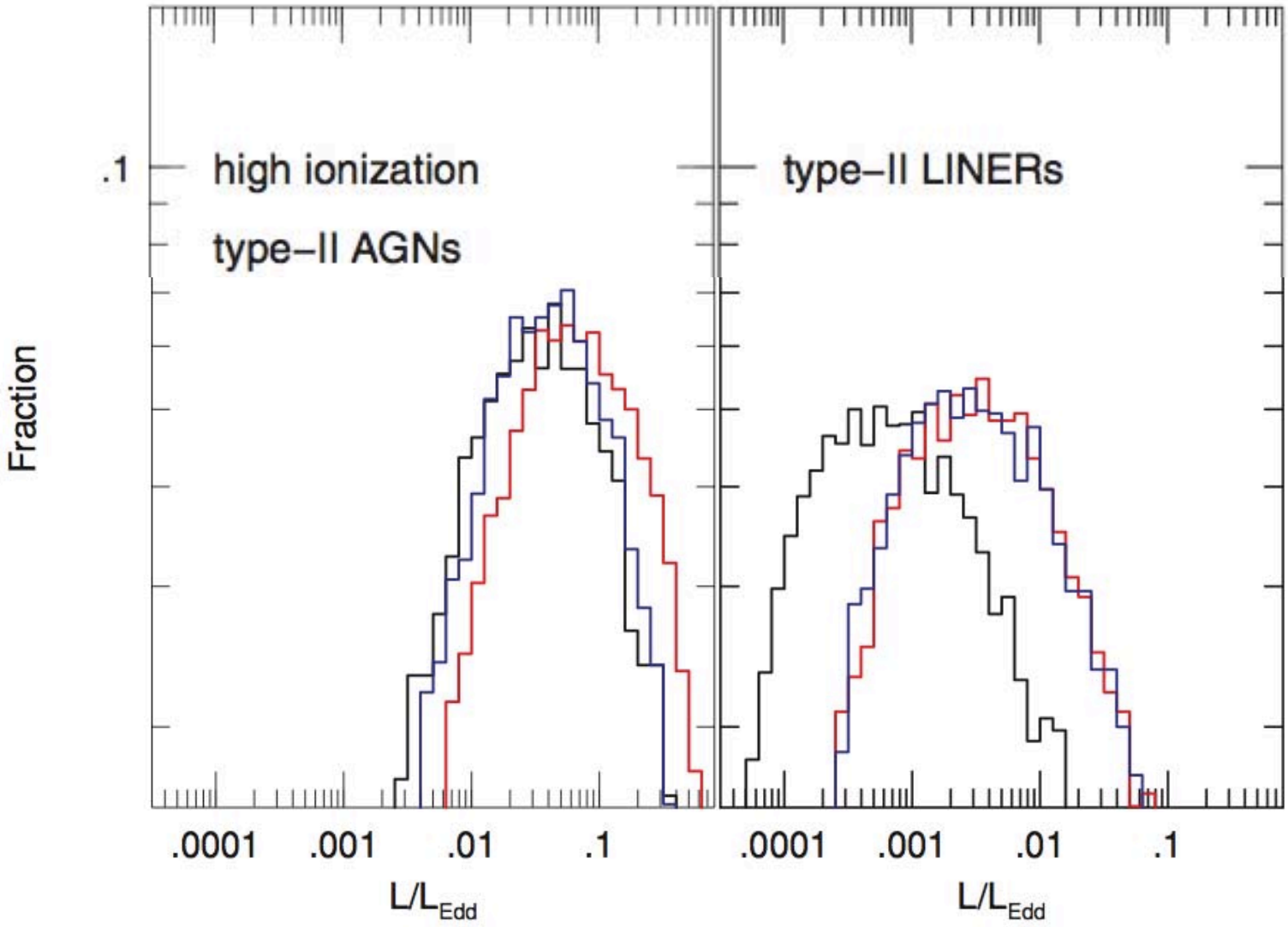

Figure 7.26. $L/L_{\rm Edd}$ distributions for $z < 0.1$ type-II AGNs as marked. The estimates are based on $L(\rm H\beta)$ (red curves), $L(\rm O\,III)$ (black curves), and the combined luminosity of O III and O I (blue curves). All methods agree very well for high-ionization sources, but the O III method underestimates $L_{\rm bol}$ and hence $L/L_{\rm Edd}$ in the low-ionization LINERs (adapted from Netzer, 2009).

NLR Relation to Bulge

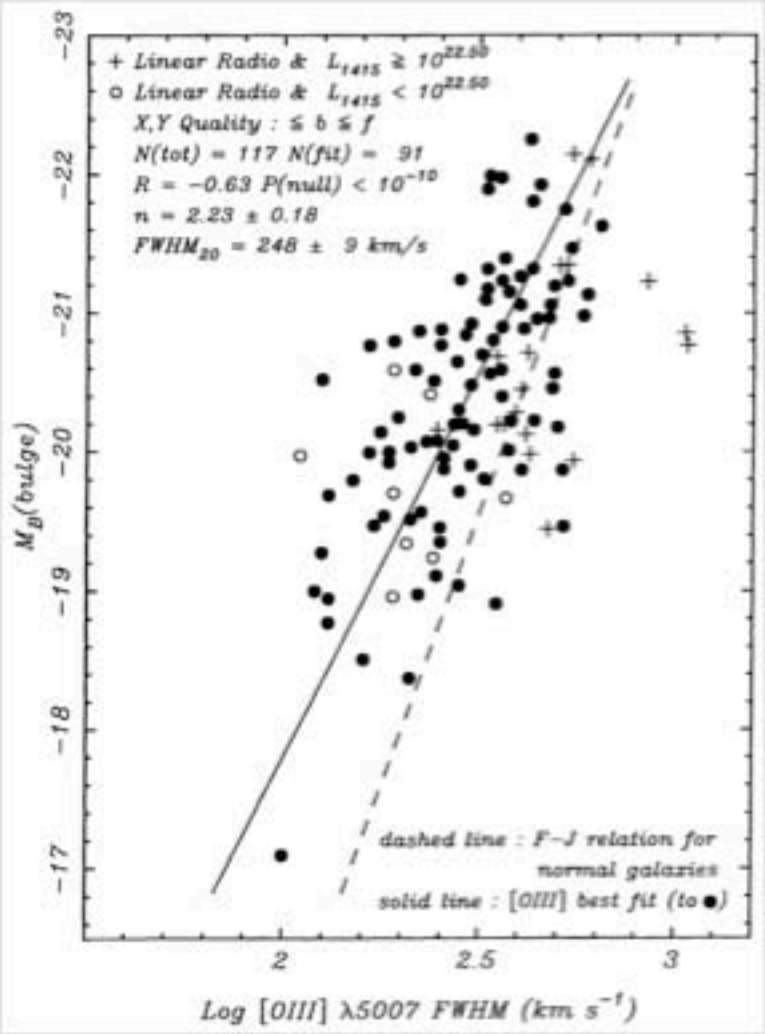

Whittle (1992)

NLR line widths are correlated with host-galaxy bulge luminosity (and bulge gravitational potential).

Indicates NLR widths are primarily virial in origin, reflecting the gravitational field of the stars (and not the black hole).

AGNs with powerful radio jets lie off the correlation, having larger widths than expected.

Apparently can also be some non-virial component to the velocities, such as shock interactions between the radio jets and NLR gas.

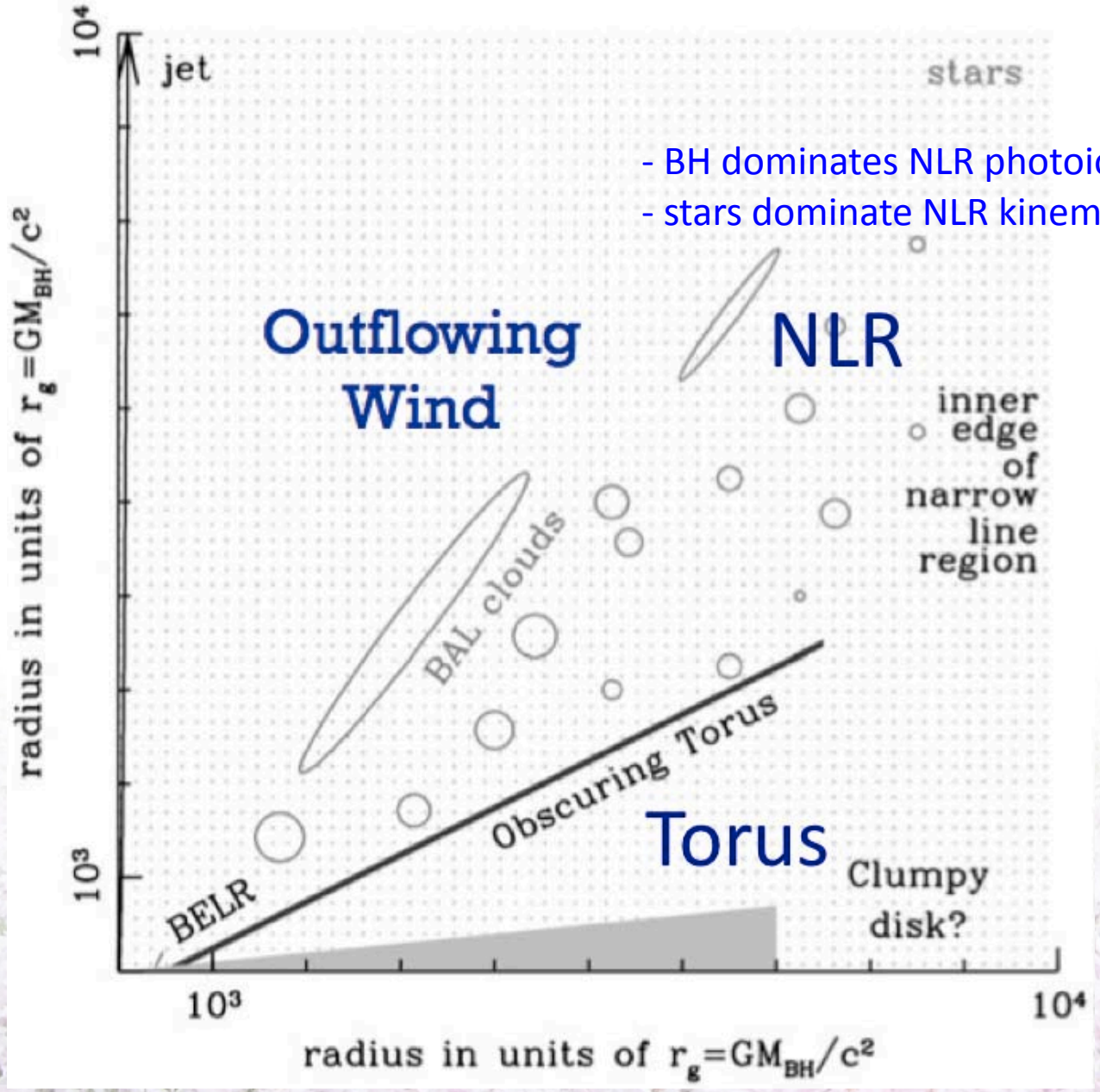

- BH dominates NLR photoionization
- stars dominate NLR kinematics

NLR Line Profiles

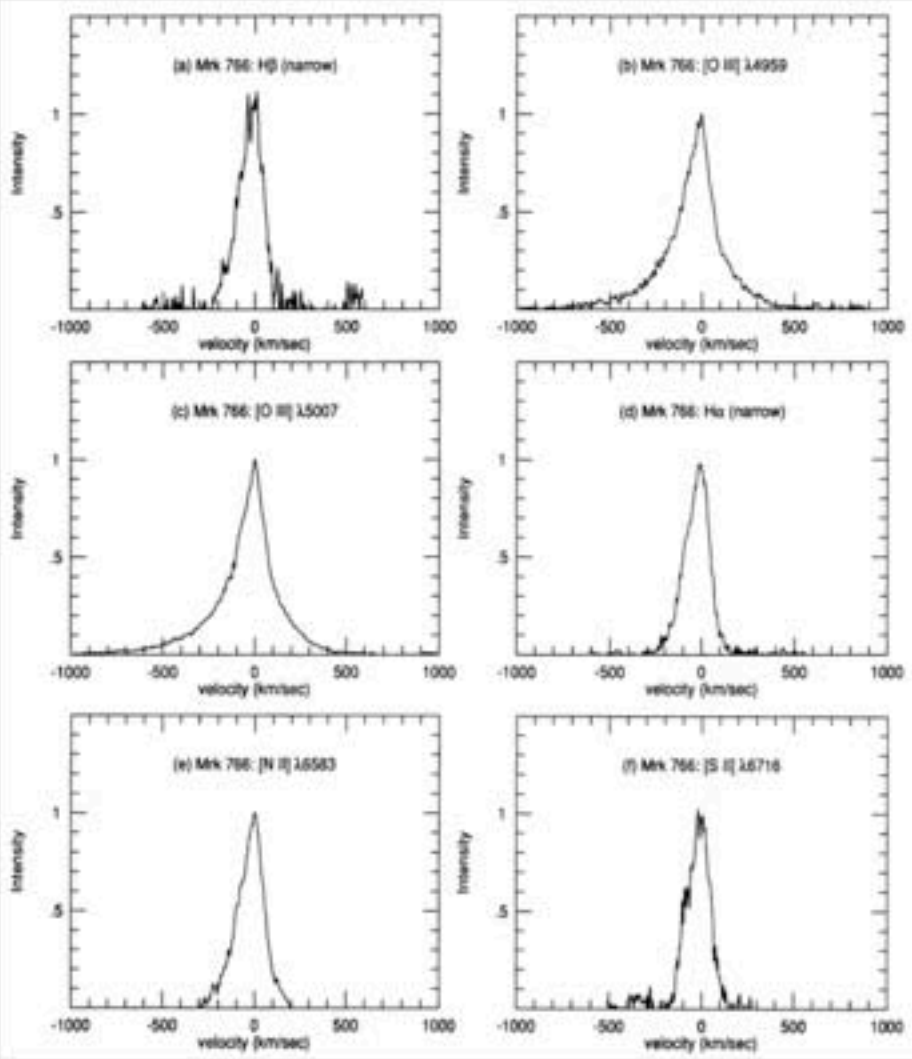

Veilleux (1991)

NLR line profiles are non-Gaussian

- Stronger bases than Gaussian
- Often blueward asymmetric, especially in the line base

Asymmetry arises from some combination of outflow motion plus dust extinction.

Redshifted side of outflow extincted, leading to the line asymmetry.

This is also seen in direct NLR mapping.

In a given object, NLR line widths are larger for higher ionization species; radial stratification of the NLR.

Flux and Velocity Maps of Brγ

(n=7 → n=4)

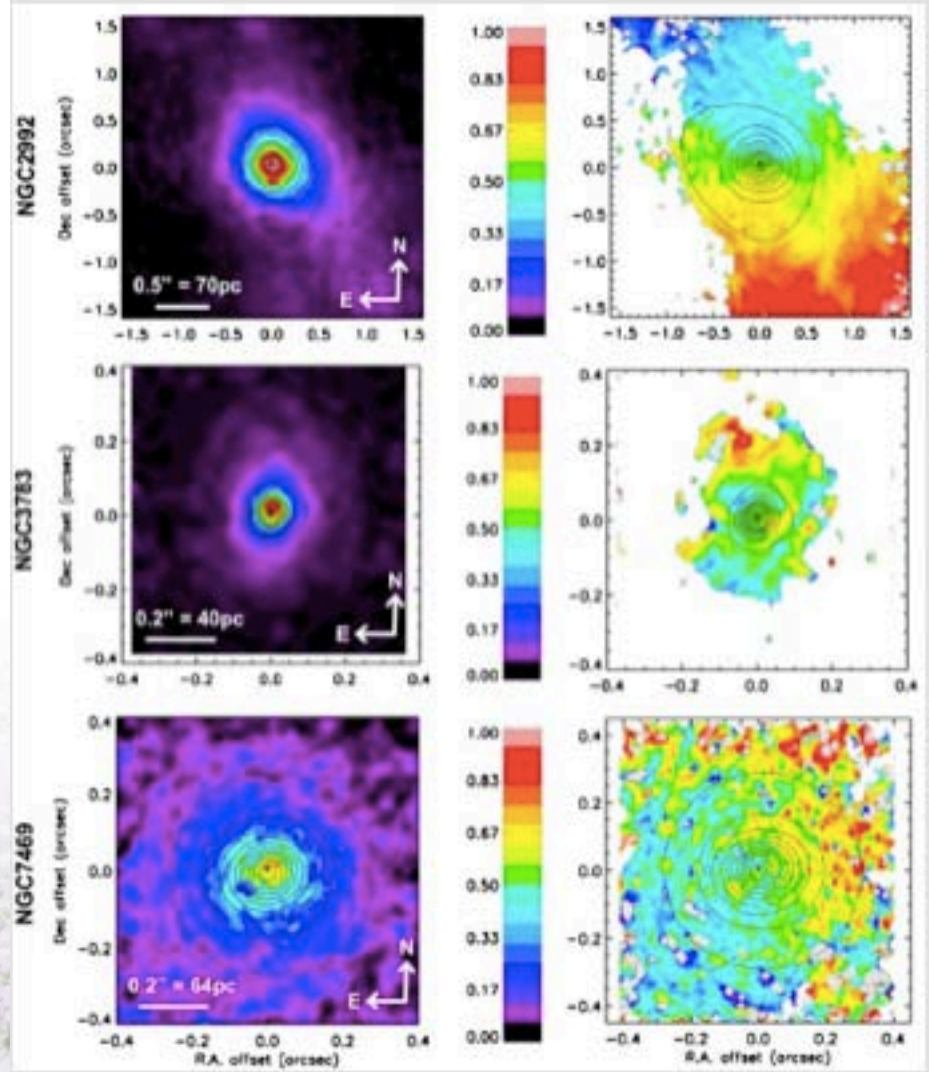

2.1655 μm, thereby minimizing extinction

Sometimes see ~ biconical outflow signatures

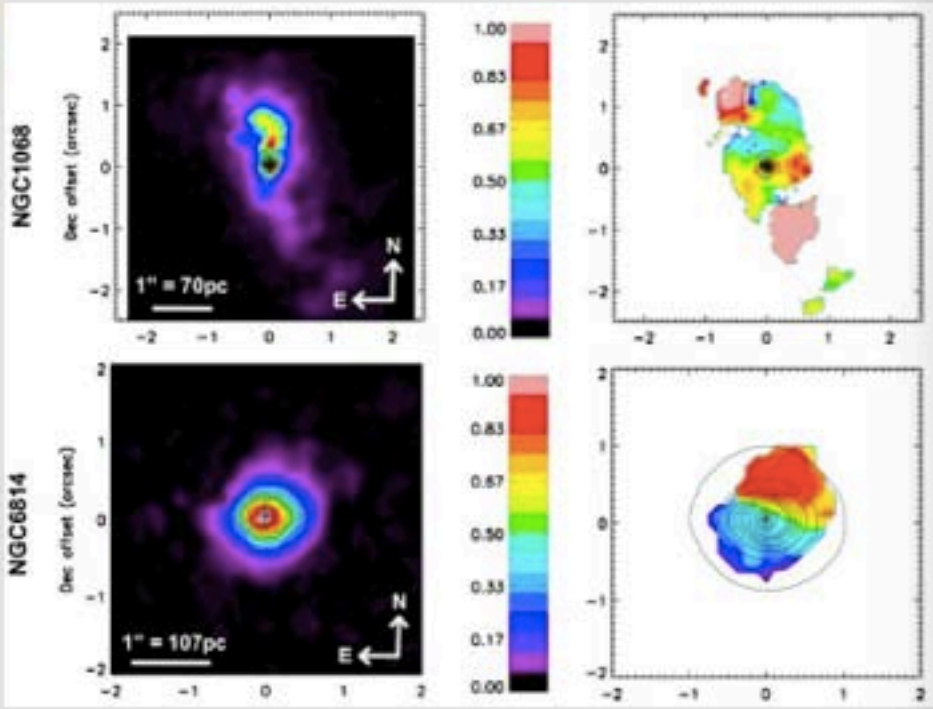

Muller-Sanchez et al. (2011)

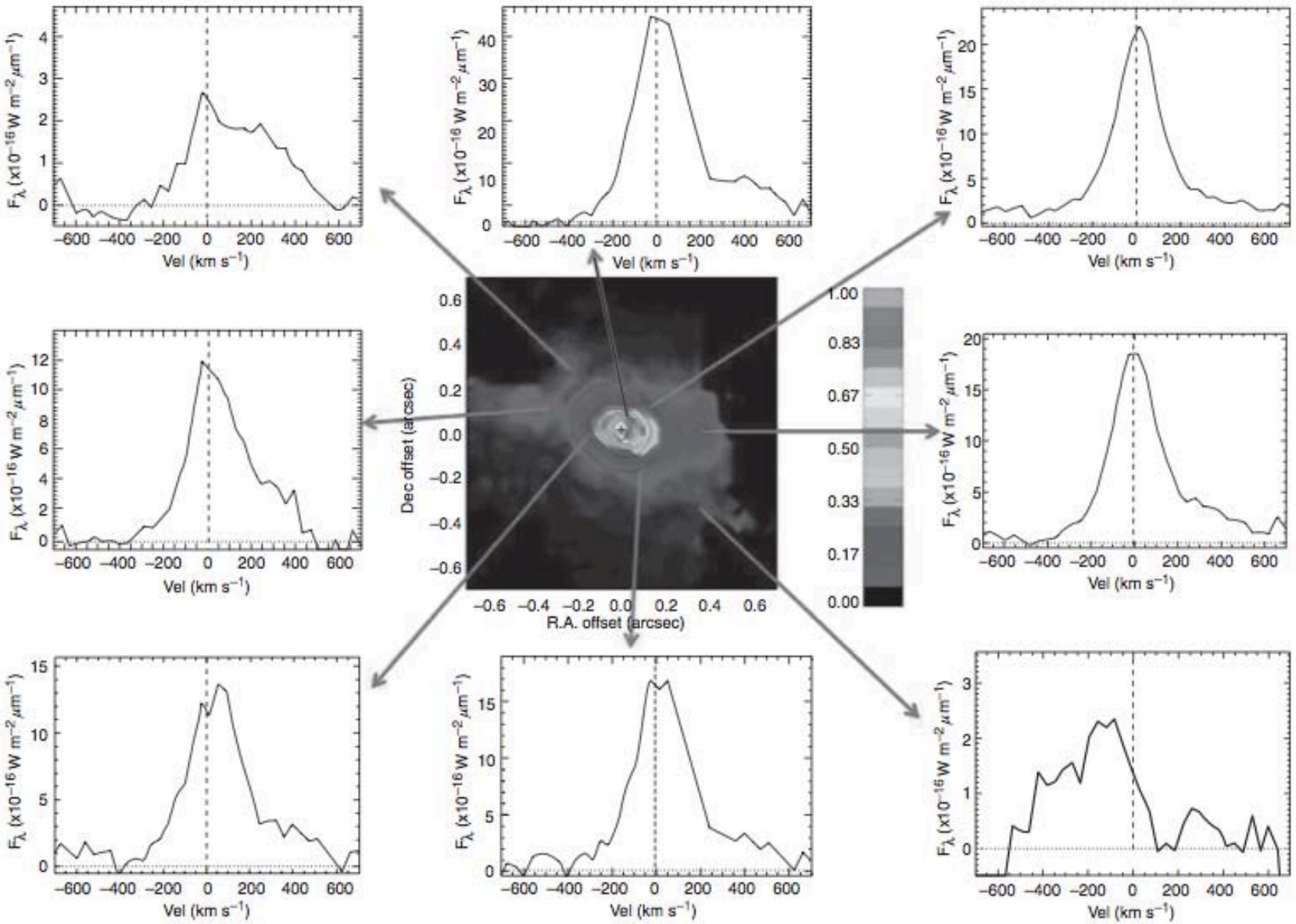

Figure 7.23. IFU map of the type-I source NGC 4151 in the light of the coronal line [SiVI] 1.96 μm. The central panel shows a flux map of the line, and the velocity information is shown as various line profiles in the different parts of this region. The size of the central square corresponds to 1.2″ × 1.2″ (80 × 80 pc at the source) (courtesy of F. Meueller-Sanchez, from Meuller-Sanchez et al., 2011; reproduced by permission of the AAS).

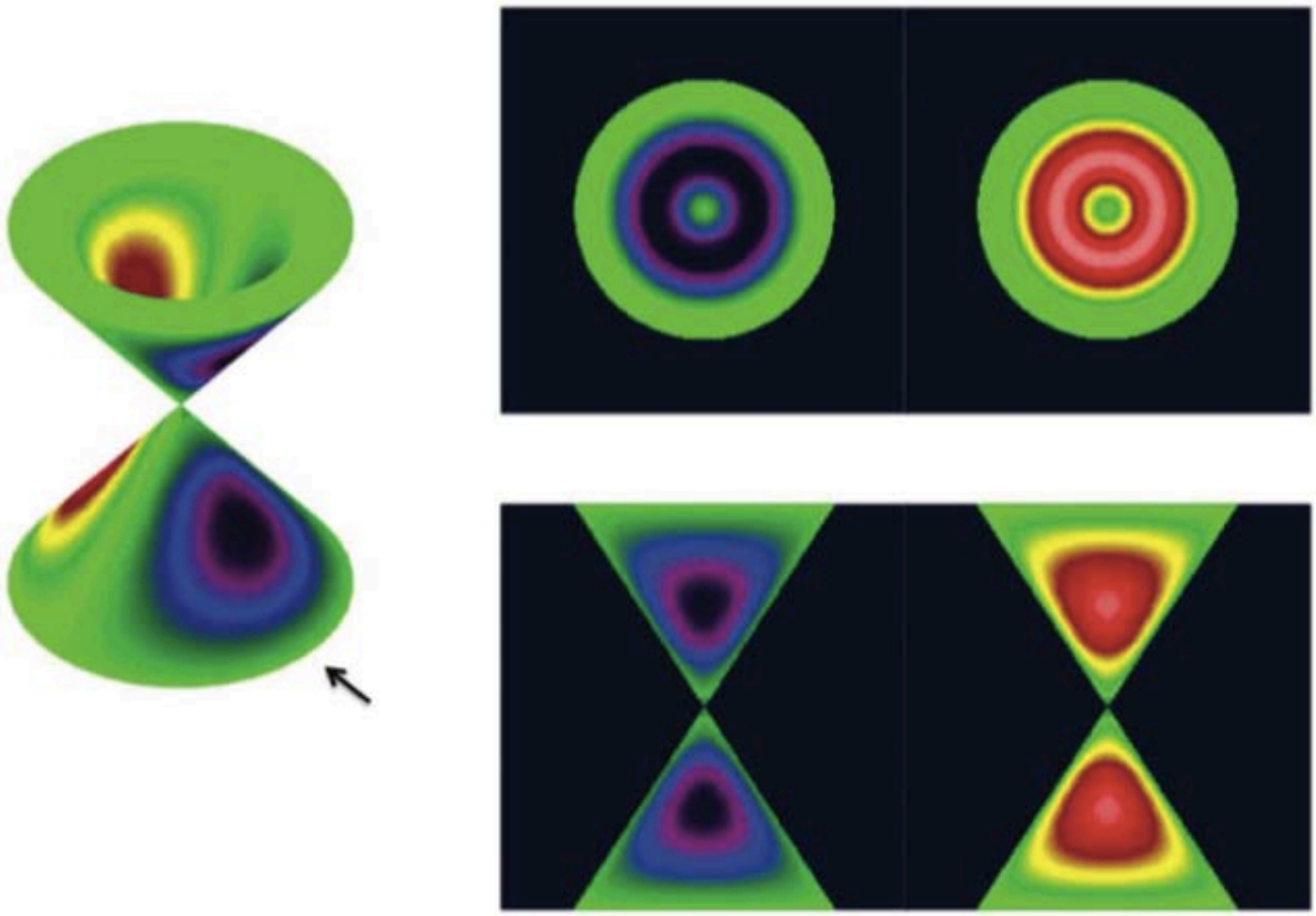

Figure 7.24. An example of a bicone model of outflow velocity field. (left) Three-dimensional structure of the model with the arrow indicating the line of sight. (top right) Front and back projections for inclination angle 90°. (bottom right) Bicone angle of 0°. The velocities are indicated by the colors, with warm colors showing the amount of redshift and cold colors the amounts of blueshift. Green represents approximately zero velocity (courtesy of F. Meueller-Sanchez, from Meuller-Sanchez et al., 2011; reproduced by permission of the AAS). (See color

Ionization Cones

Often see "ionization cones" in maps of high-excitation lines; wedge-shaped structures of gas ionized by the AGN continuum.

These often begin in the "classical" NLR, and can extend outward to ~ kpc scales, forming an "extended" NLR.

The fairly sharp edges of ionization cones are defined by the collimation of light from the AGN.

Collimation could be due to "shadowing" by the torus, or alternatively an inherently anisotropic ionizing continuum.

They come in single-sided and bi-conical types, with the single-sided ones presumably having an obscured counterpart on the other side.

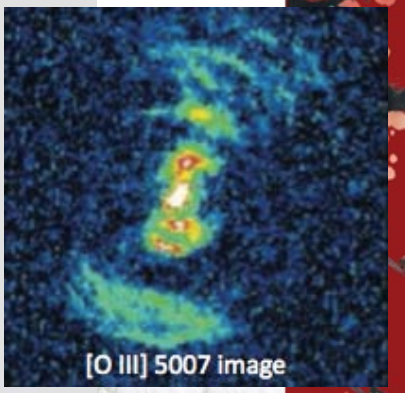
[O III] 5007 image

Why Distinct BLR + NLR?

Line EWs from "Clouds" at Different Radii

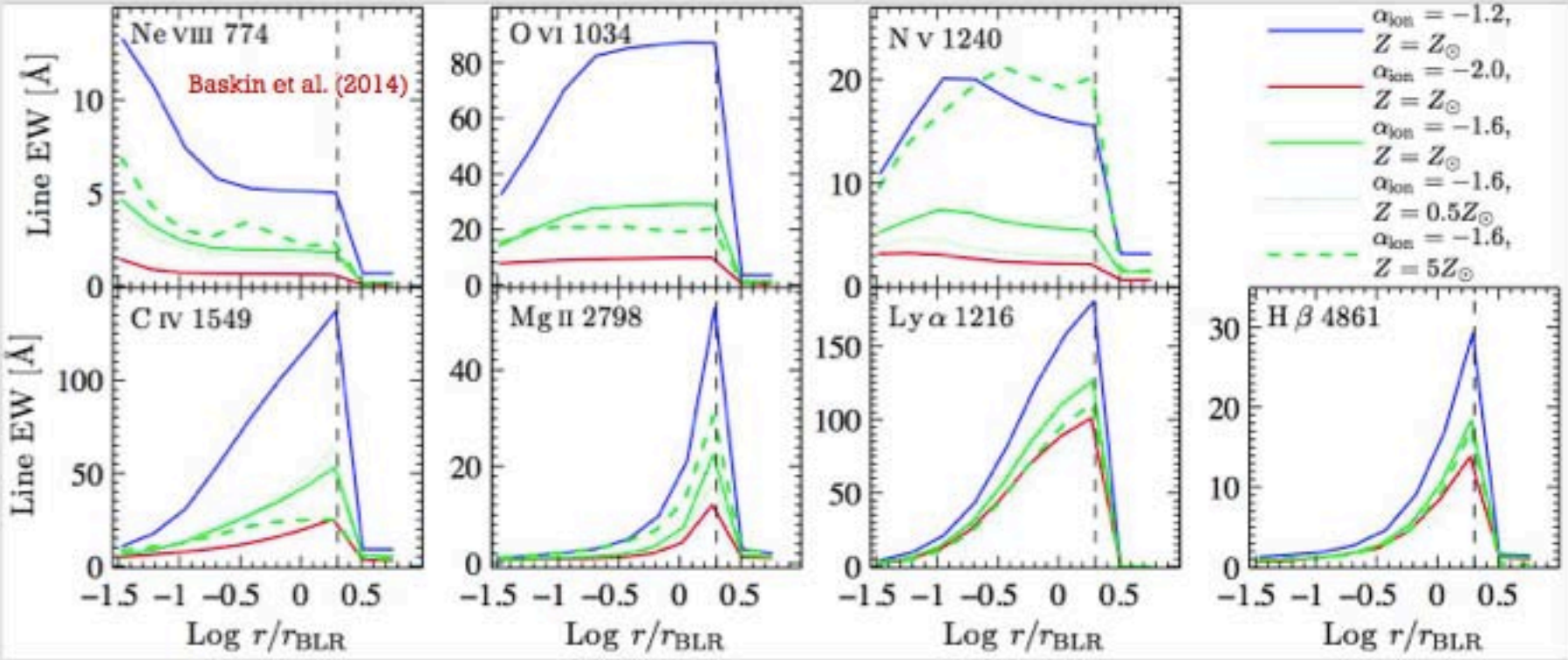

Beyond the dust sublimation radius (vertical dashed lines), about 80% of incident radiation is re-radiated by dust in the infrared.

The line emission drops sharply when dust is present, and then must go far out to accumulate sufficient emission from NLR gas. This is the likely cause of the distinct BLR + NLR structure.

Stars and starburst regions

Stars and starburst regions

- Bloated stars in nuclear cluster also absorb and reprocess incident AGN radiation and are hence potential sources of emission lines
  - some non-MS stars may develop extended winds/envelopes as a result of interaction of their atmosphere with the hard, external AGN radiation field
  - star-star collisions may also produce bloated stars
  - bloated stars' extended envelopes similar to low-density gas in many ways
    * can show a typical BLR/NLR spectrum depending on distances
    * such stars can also provide another reservoir for the emission-line gas
- Starburst regions in AGNs
  - different from other AGN components because of their dimension (up to several kpc), location, main source of E (radiation of young massive stars and mechanical E from SN explosions and fast stellar winds)
  - optical signatures can be differentiated by line-ratio diagnostic (BPT) diagrams
  - X-ray signatures (~1e7 K) from a multi-temperature hot plasma that contains strong collisionally excited emission lines (cf. AGN gas <~1e5 K)
  - some show a mixed-type spectrum as being exposed to AGN radiation

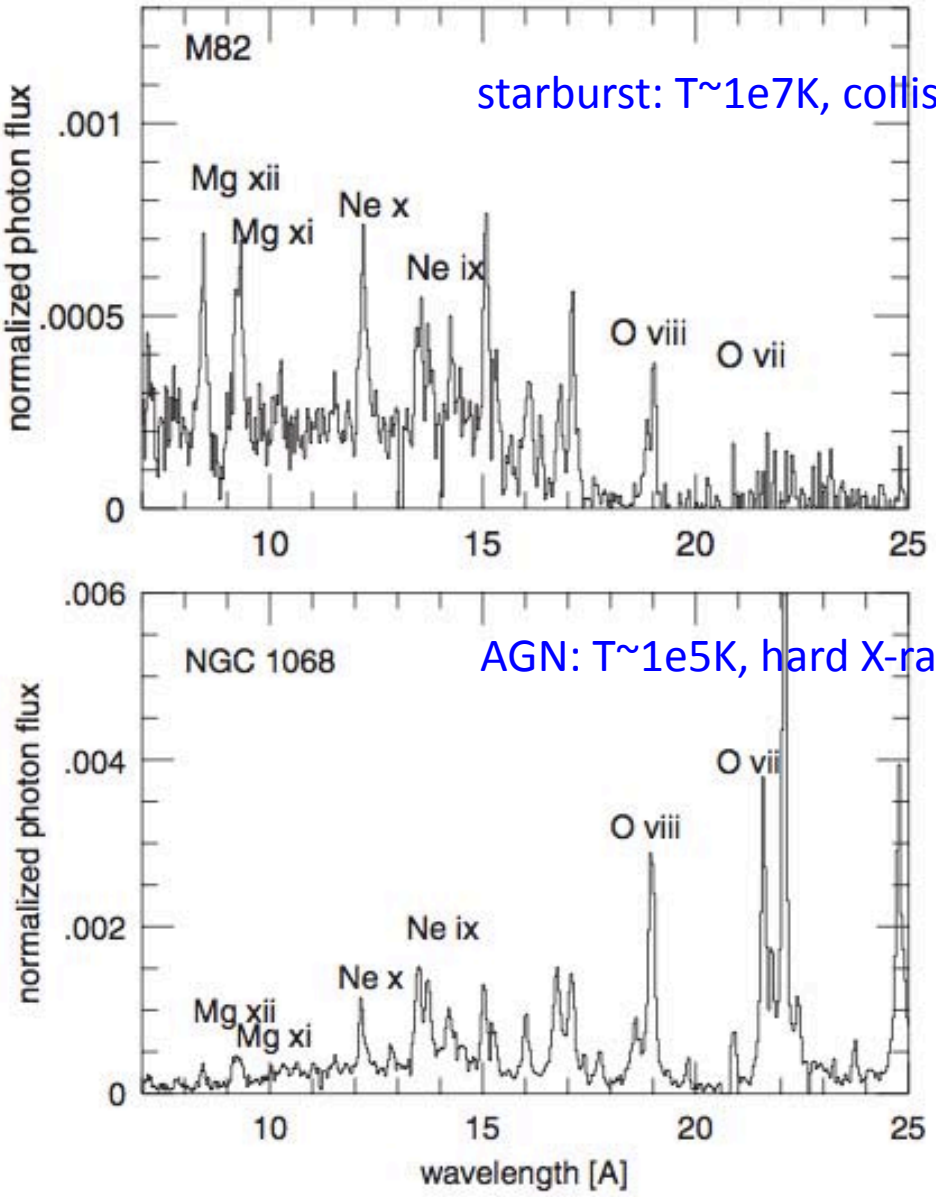

starburst: T~1e7K, collisionally ionized

AGN: T~1e5K, hard X-ray photonionized

Figure 7.38. A comparison of X-ray photoionized gas (NGC 1068, a type-II AGN with an extended X-ray nebulosity) and X-ray collisional gas (M82, a "classical" starburst galaxy). Both spectra were obtained by the RGS on board XMM-Newton and were retrieved from the XMM archive.

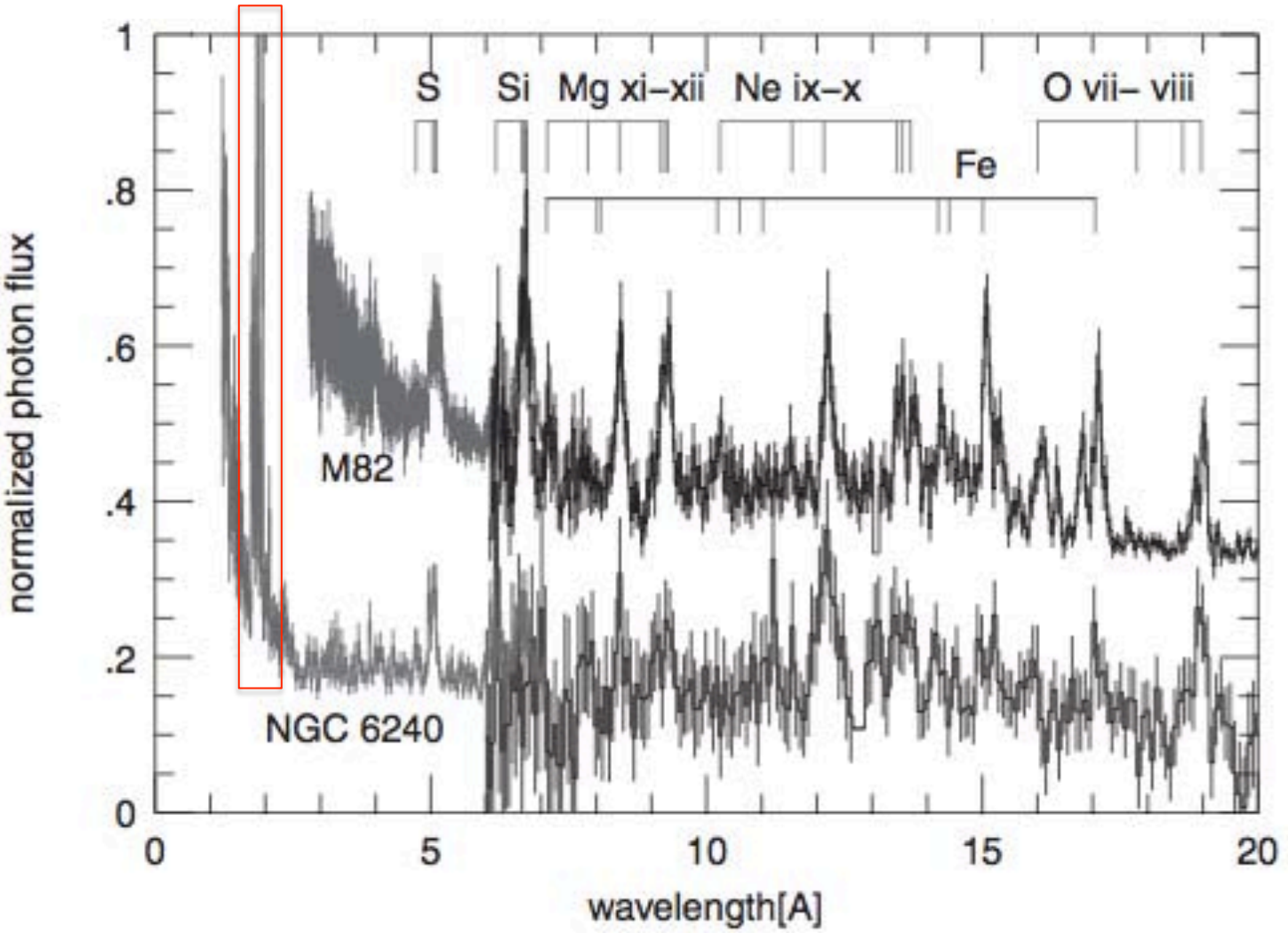

Figure 7.39. A comparison of the X-ray spectra of the SB galaxy M 82 and the double-nucleus AGN ULIRG NGC 6240 (adapted from Netzer et al., 2005). The similar soft X-ray emission-line spectra of the two sources are typical of collisionally ionized plasma. The only exception is the strong Kα line at around 1.9 Å, which is seen only in the spectrum of the AGN.

Jets

The central jet

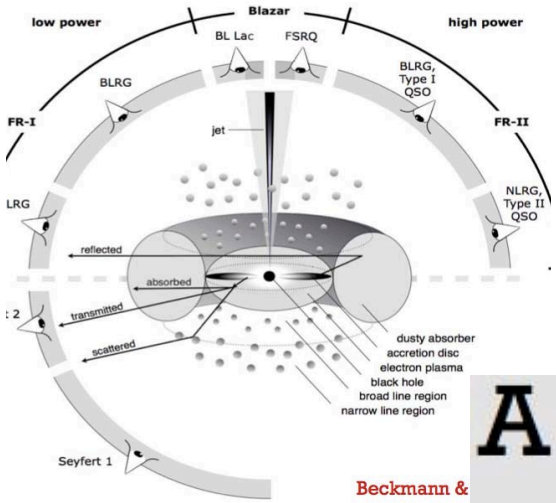

Beckmann &

A Useful Working Hypothesis

At least to first order, we can adopt many of the findings about radio-quiet AGNs for radio-loud AGNs.

RL AGN ~ RQ AGN + Strong Jets

For example, they have accreting SMBHs, they have BLRs, they have NLRs, etc.

A tremendous simplification, and often seems to work well to first order of approximation (but not to higher orders).

Radio-Loud AGNs

AGNs are often divided into radio-loud vs. radio-quiet using

$$R = L_\nu(5\ \mathrm{GHz}) \,/\, L_\nu(4400\ \mathrm{A})$$

where $R = 10$ is the typical (arbitrary) separator value.

About 10% of luminous AGNs are radio loud.

But no strong R bimodality, and perhaps none at all.

Even nominally radio-quiet quasars can have weak jets.

Radio-loudness is generally associated with strong particle jets emitting a synchrotron power-law continuum in the radio.

Radio-Loud vs. Radio-Quiet SEDs

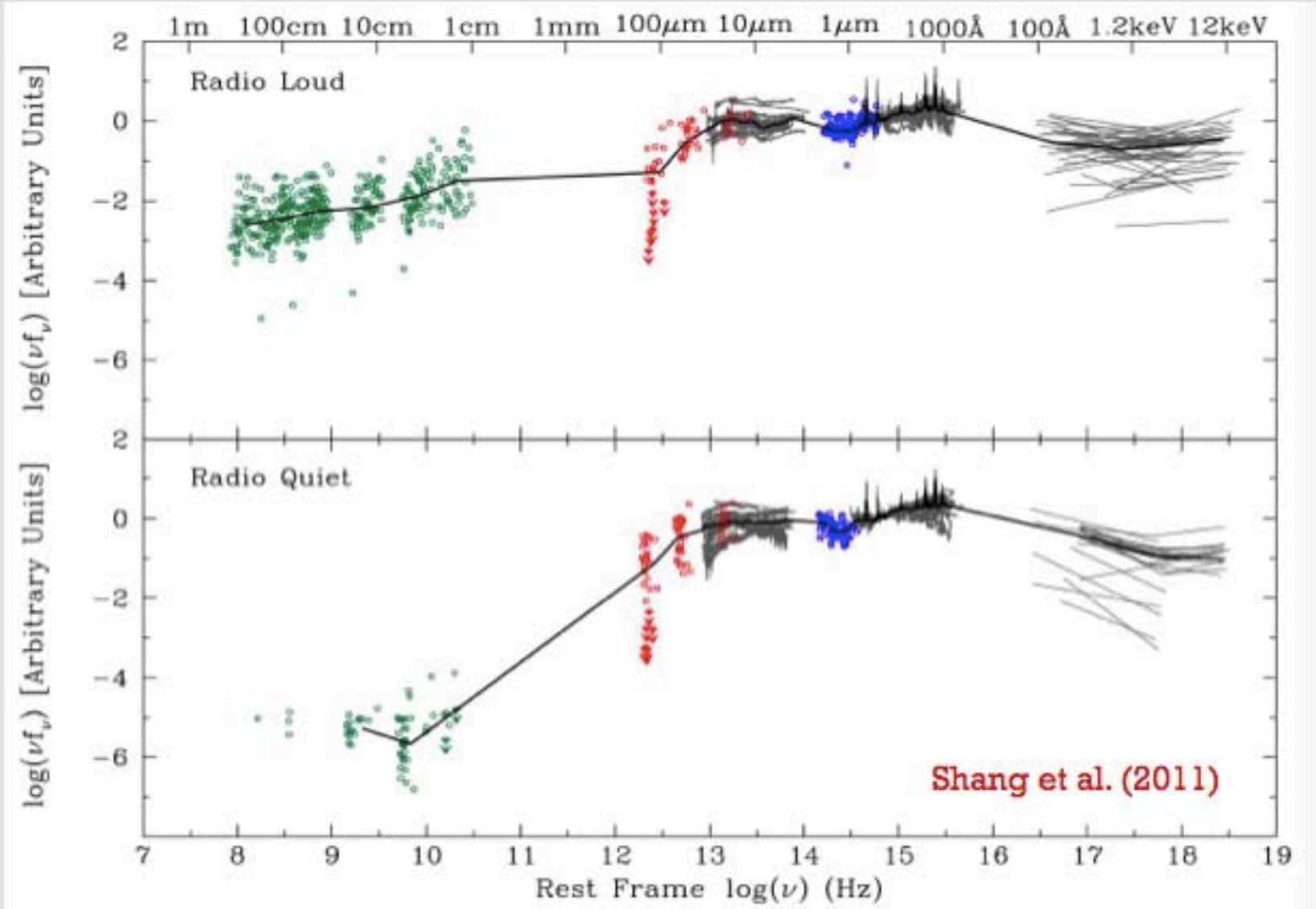

Components of a Radio Source

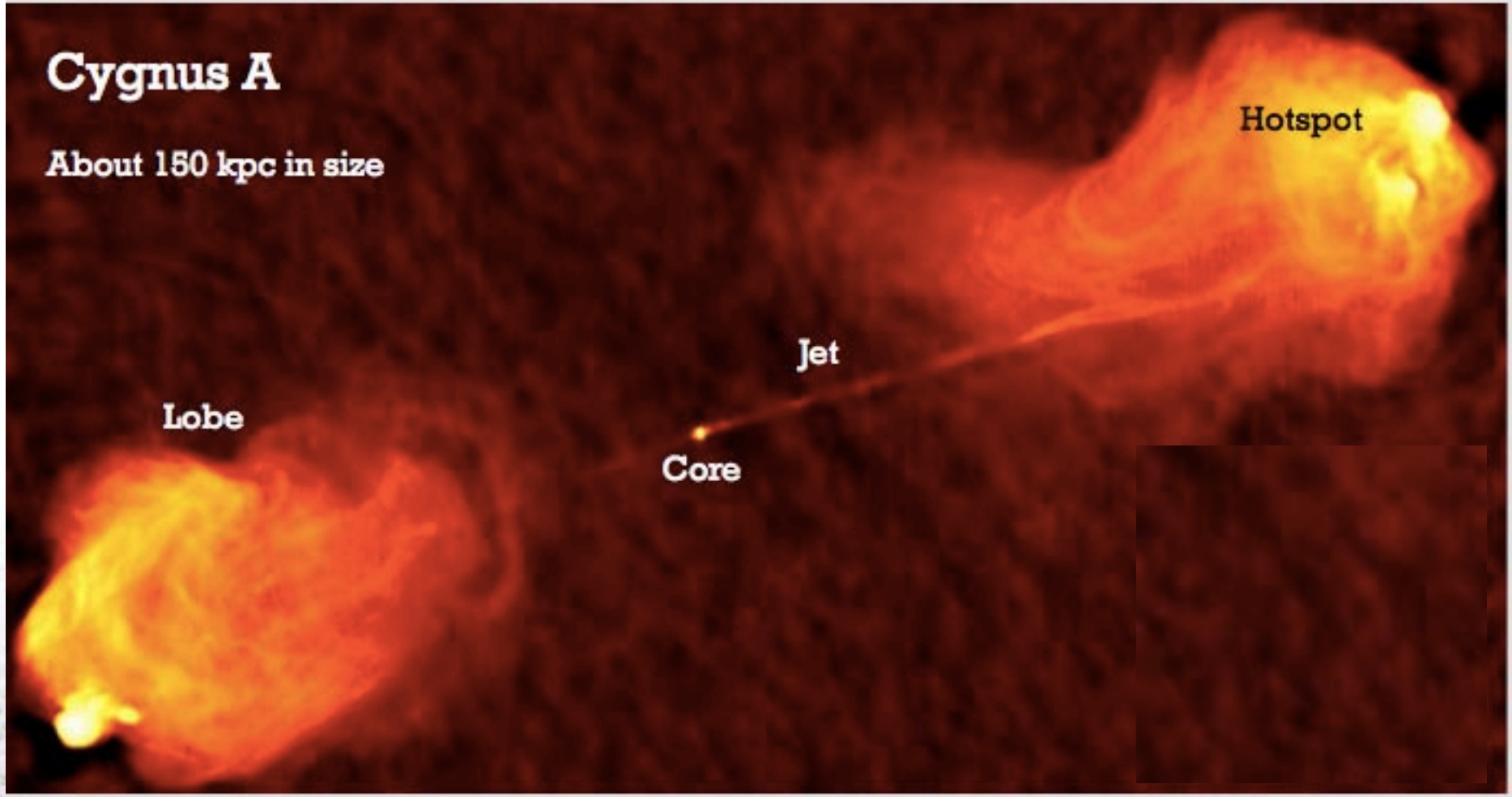

Carilli & Barthel (1996)

A 3 Mpc Size Radio Galaxy

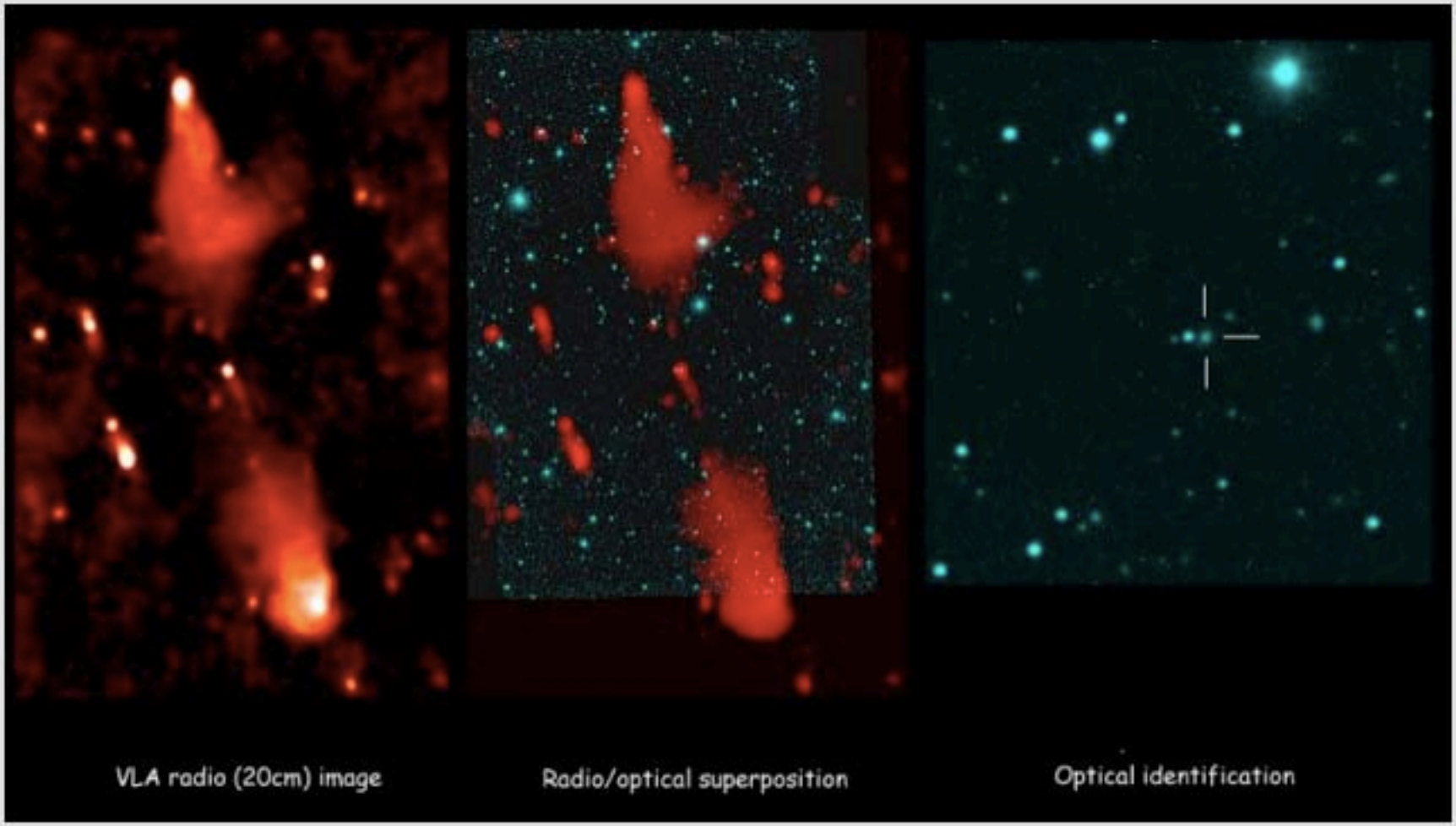

Palma et al. (2000)

Diverse Radio AGN Morphologies

Radio Galaxy Images at 74 MHz from the VLA Low-Frequency Sky Survey

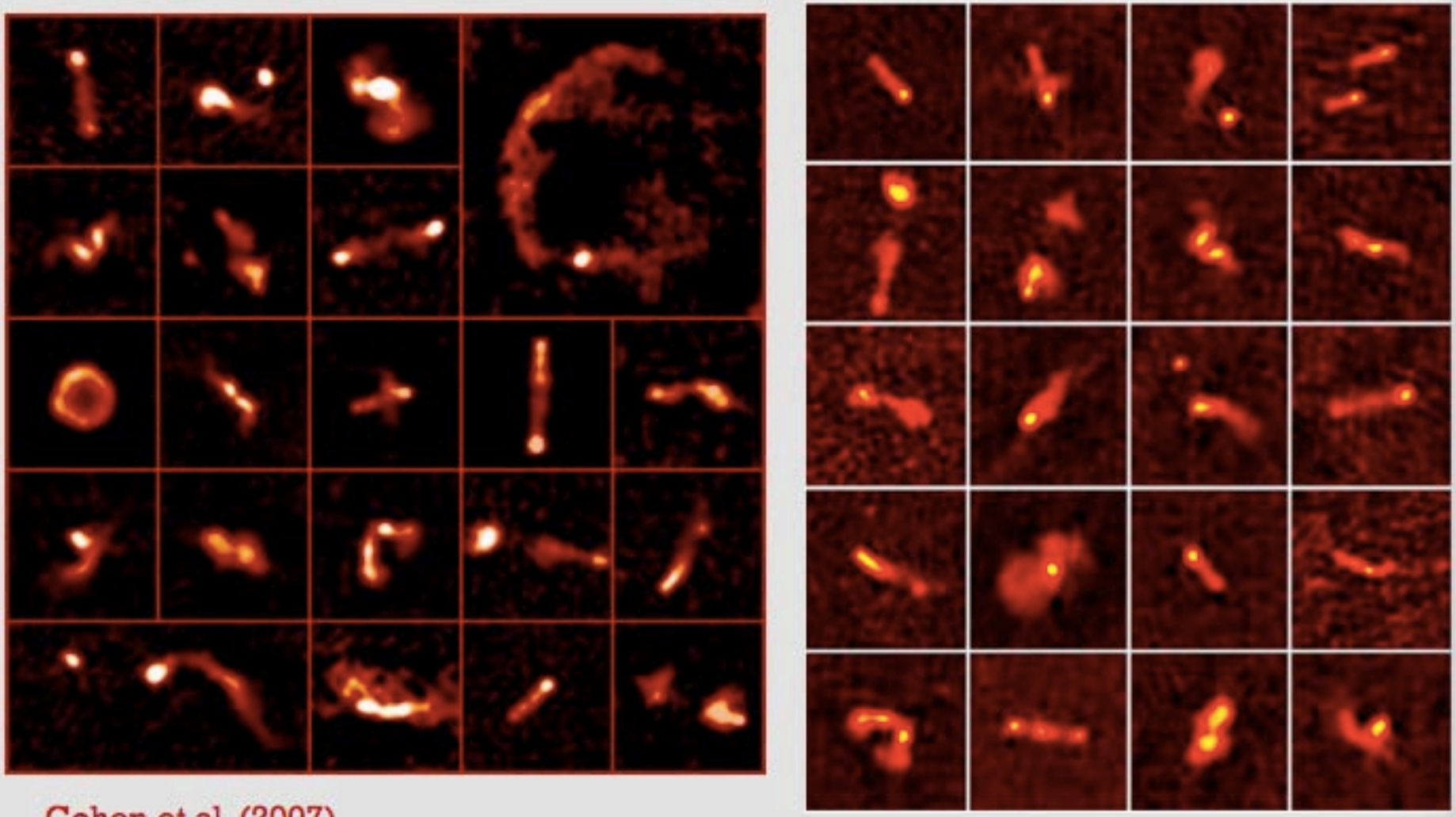

Cohen et al. (2007)

Some Basic Properties of Radio Jets

Jets often appear relativistic based on beaming, apparent superluminal motions on sub-pc scales, and variability.

Thus, the apparent properties of a jet depend *strongly* upon orientation.

At least in some cases, jets are launched on very small scales (making much of the "core" radio emission). And they can be collimated over a huge range of scales.

Jets are often seen in the X-ray and also the optical.

Superluminal Motion in the M87 Jet

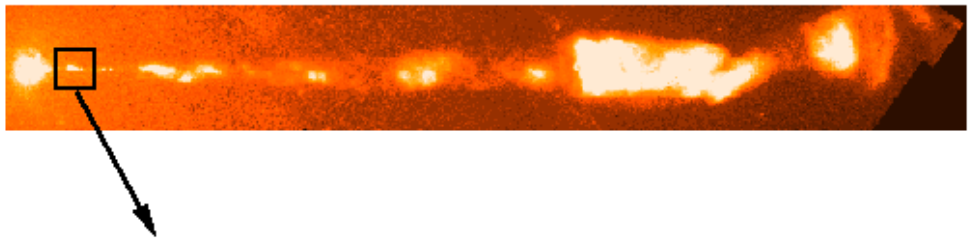

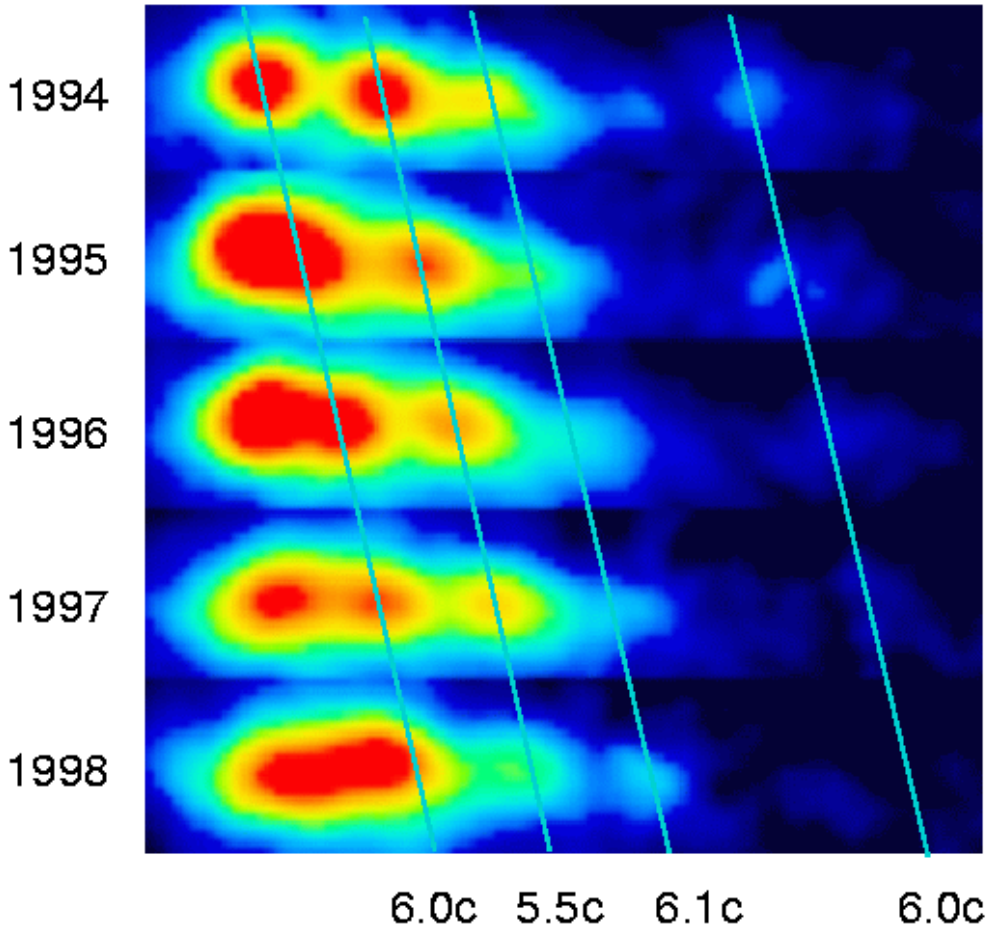

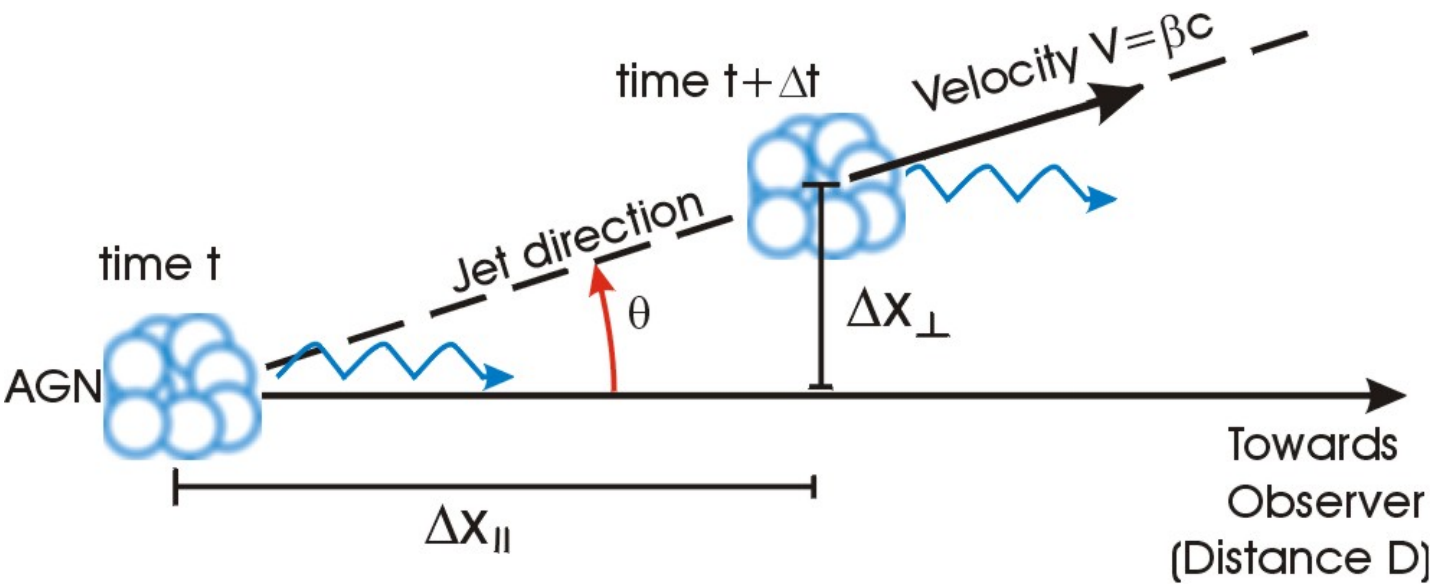

$$\Delta x_{\parallel} = \beta c \Delta t \times \cos\theta$$

$$\Delta x_{\perp} = \beta c \Delta t \times \sin\theta$$

$$\Delta t_{\text{obs}} = \Delta t - \frac{\Delta x_{\parallel}}{c} = \left(1 - \beta \cos\theta\right) \times \Delta t$$

$$\left(V_{\perp}\right)_{\text{app}} = \frac{\Delta x_{\perp}}{\Delta t_{\text{obs}}} = \frac{\beta c \sin\theta}{1 - \beta \cos\theta}$$

Launching of the M87 Jet

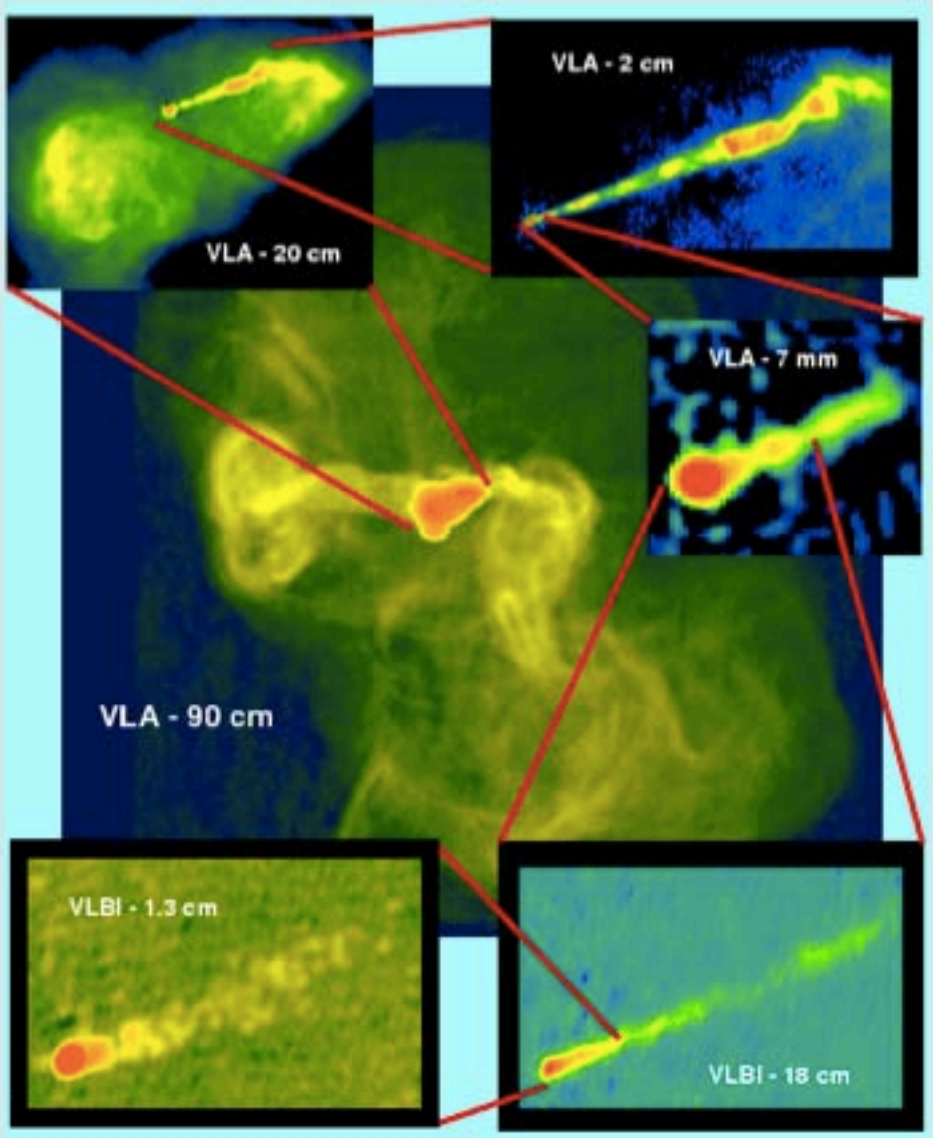

We can directly observe the M87 jet down to a few hundred R_S.

Optical Jet Emission from 3C273

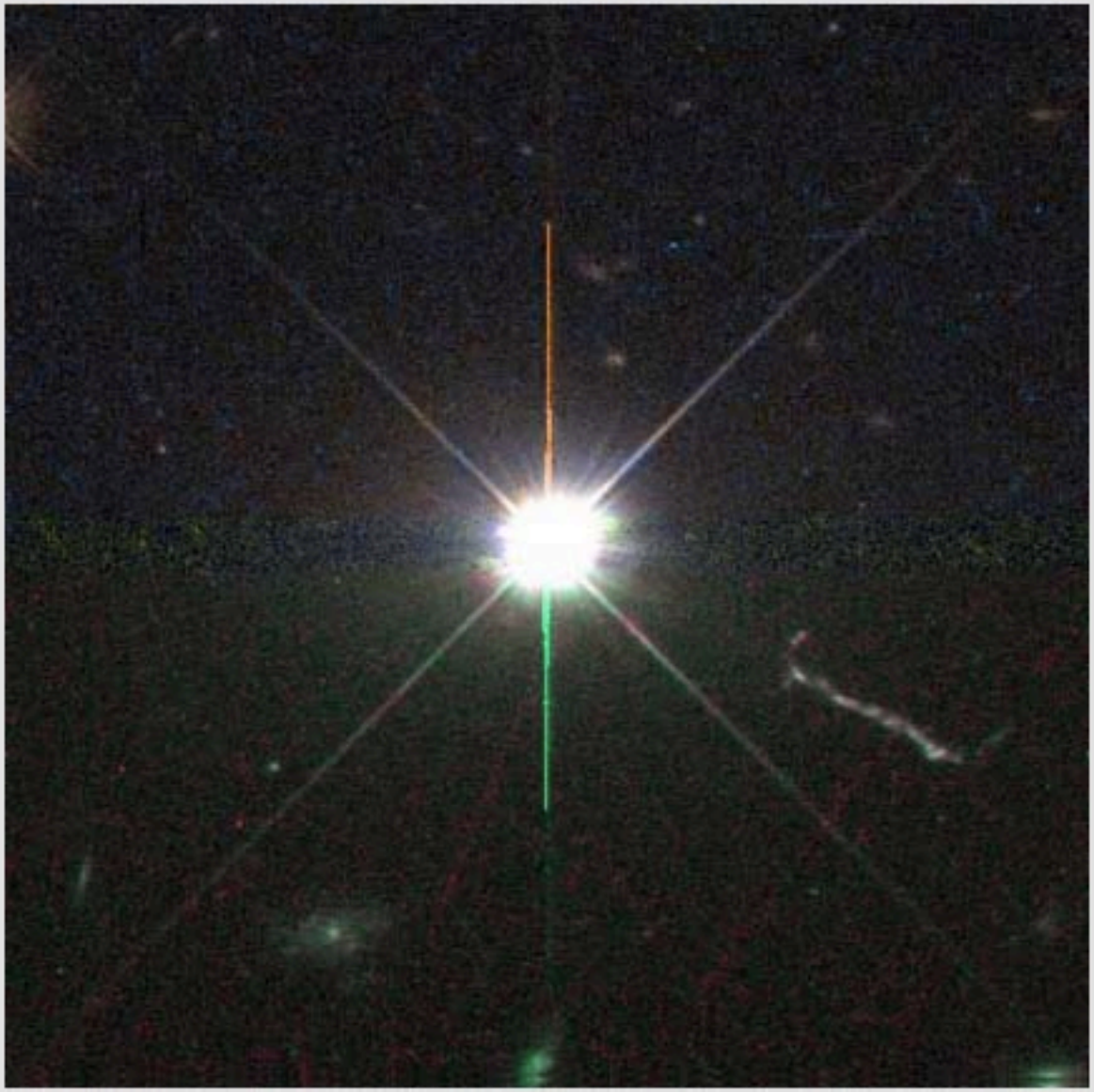

Multiwavelength Jet Emission

M87

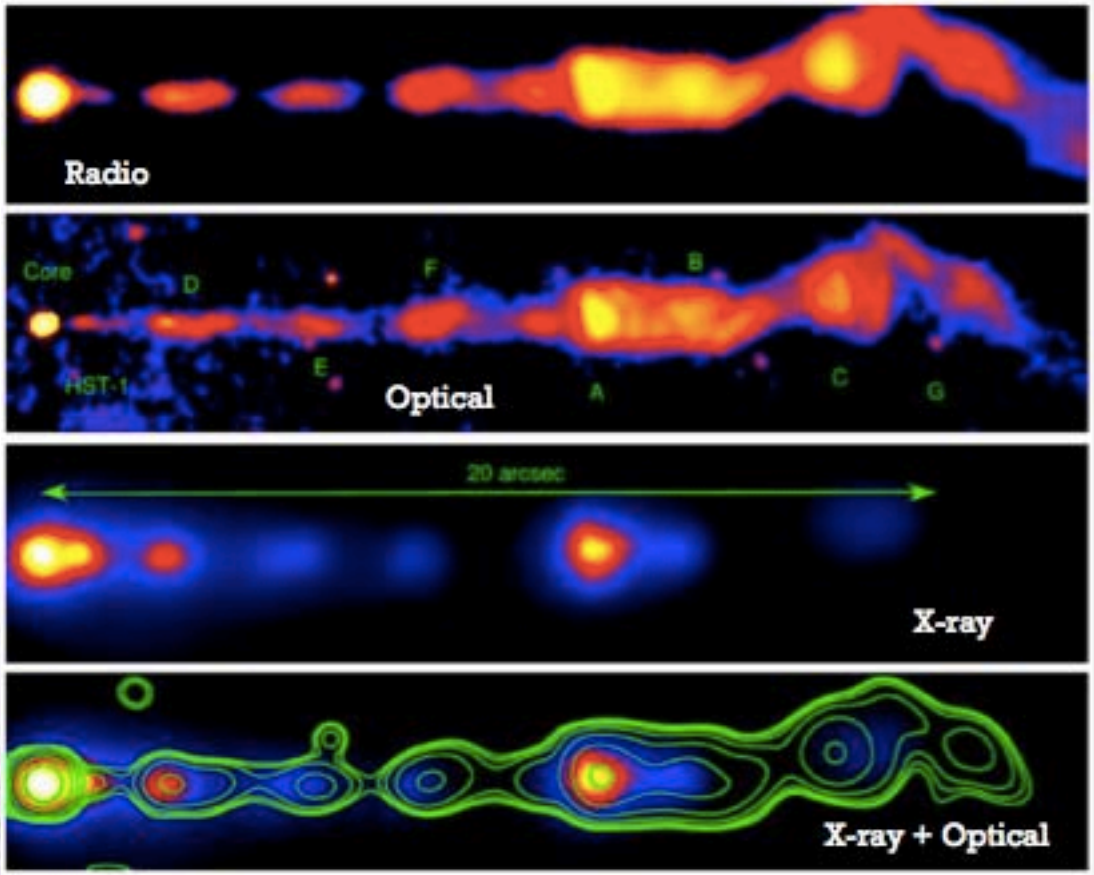

Marshall et al. (2002)

3C273

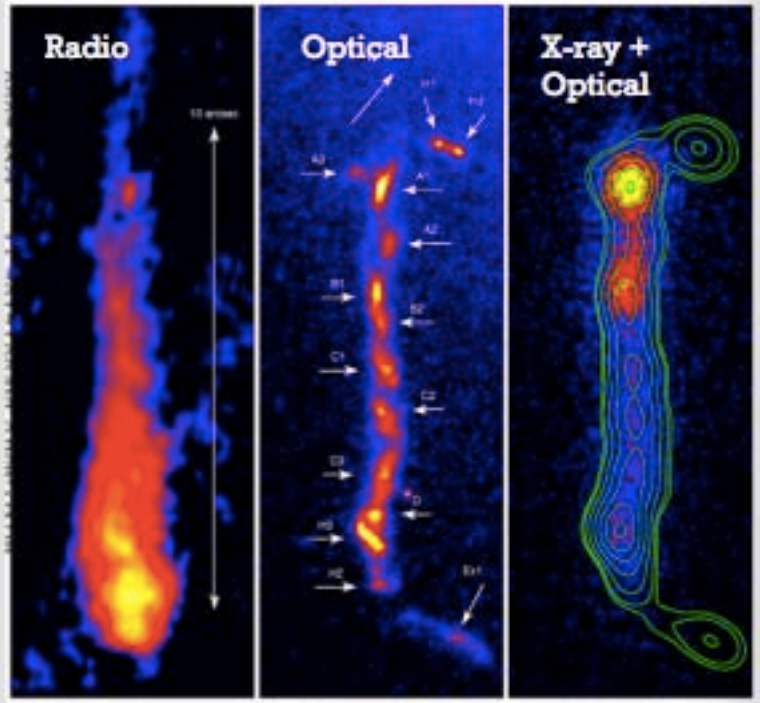

Marshall et al. (2001)

Multiwavelength Jet Emission

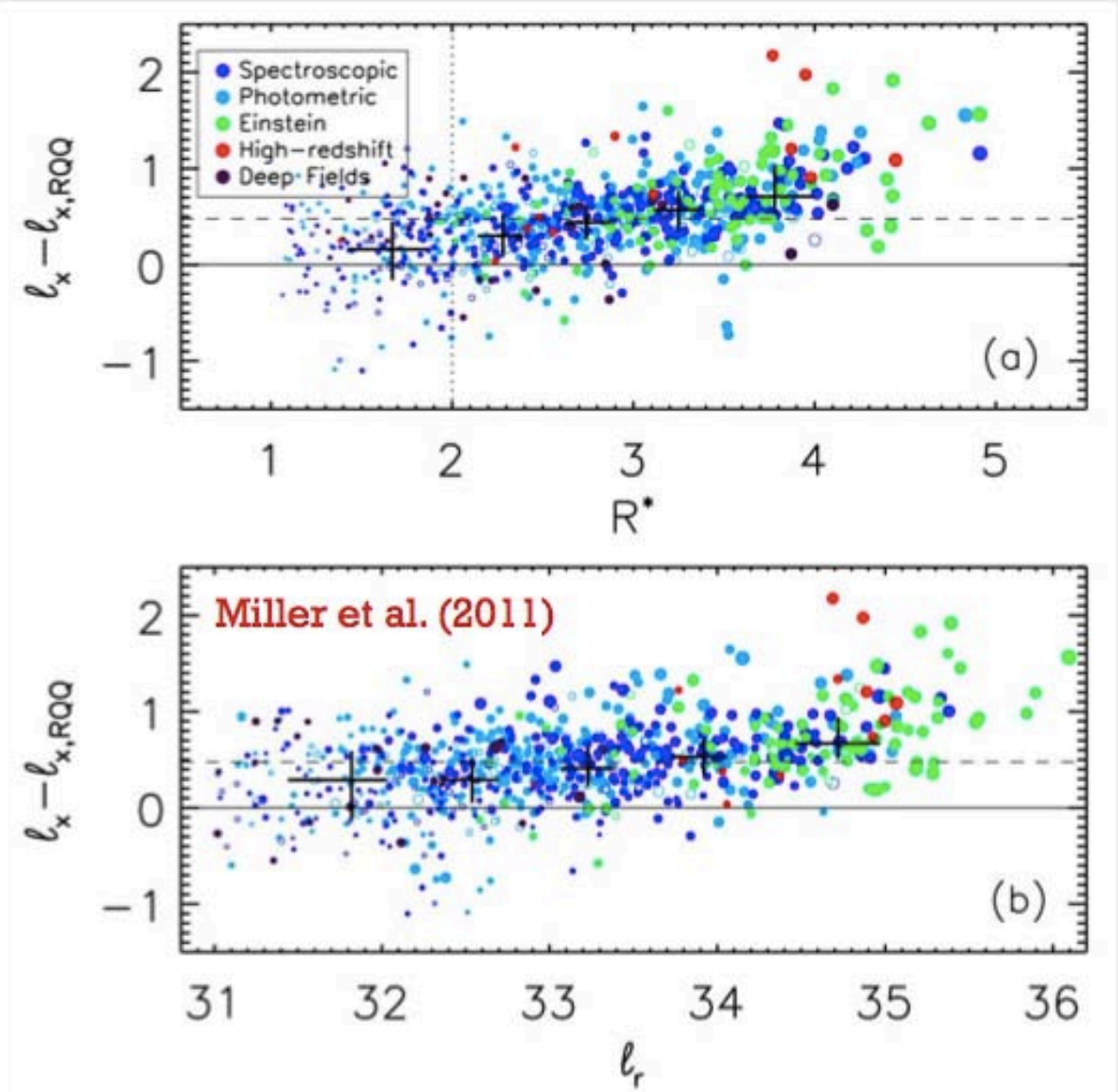

X-ray emission from radio-loud quasars increases as the radio volume control is dialed upward.

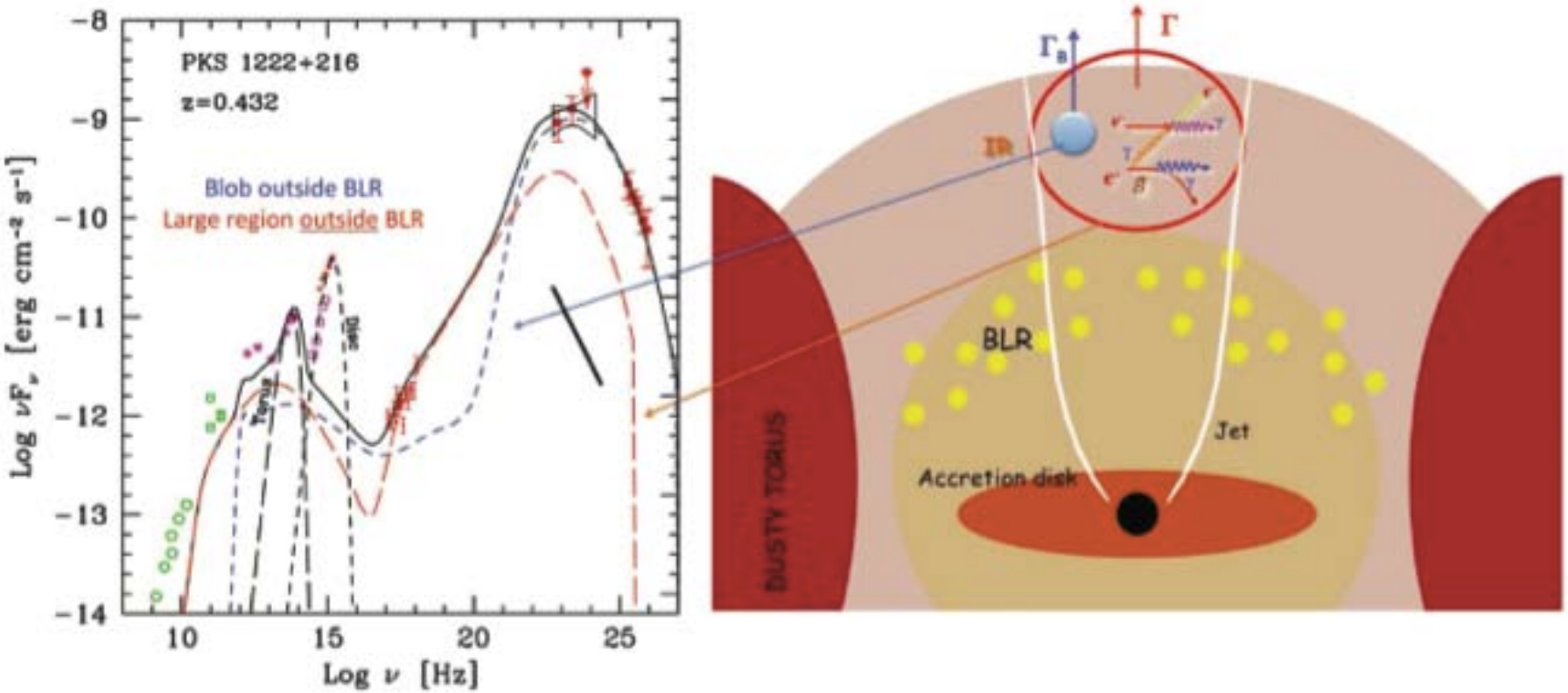

Figure 7.48. Model fit to the SED of the flat radio spectrum blazar PKS 1222+216 (from Stamerra et al., 2011; reproduced by permission of John Wiley & Sons Ltd.). Such sources have two emission peaks at low and high energies. The low-energy peak is the result of synchrotron emission. The high-energy peak is thought to be due to inverse Compton scattering of soft NIR–optical–UV photons, probably from the BLR and the accretion disk, by the relativistic electrons in the jet. The main model ingredients, with the location of the high-energy source, are shown in the right panel. The direct signature of the central torus and accretion disk, and the broad emission lines, are often seen in the spectrum of such sources (see left panel). (See color plate)

How Are Jets Made?

An accreting SMBH model has promising "ingredients" for making jets:

- Preferred axis that is stable
- Relativistically deep potential well
- Magnetic fields in orbiting plasma

Generally invoke MHD processes to divert some of the inflowing plasma outward and then keep it collimated.

How Are Jets Made?

But exactly how to combine the "ingredients" remains poorly understood.

See, e.g., Meier (2013) for a review.

What sets if a strong jet will be launched

- SMBH spin?
- Magnetic geometry?
- Environment?

Simulations of Jet Formation

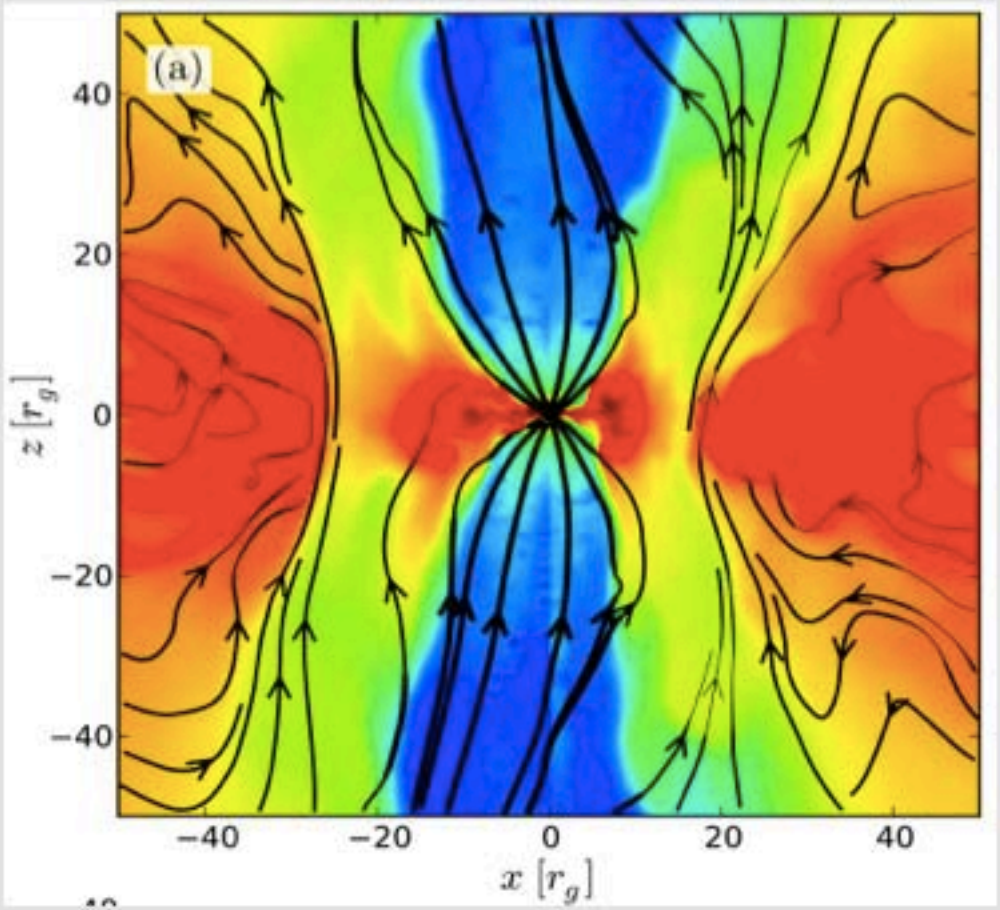

Color shows density, and black lines are magnetic-field lines.

Tchekhovskoy et al. (2012)

Simulations of accretion flows now allow the jet power to be determined as a function of SMBH spin in some regimes.

At high spins, differences found from the classical BZ formula:

$$P_{\rm BZ} = \frac{\kappa}{4\pi c}\Phi_{\rm BH}^2\frac{a^2}{16r_g^2}$$

Much work on jet formation remains, especially in the regime of high accretion rate.

Jet Feedback in Clusters

Jets can do substantial work against the hot gas in galaxy clusters

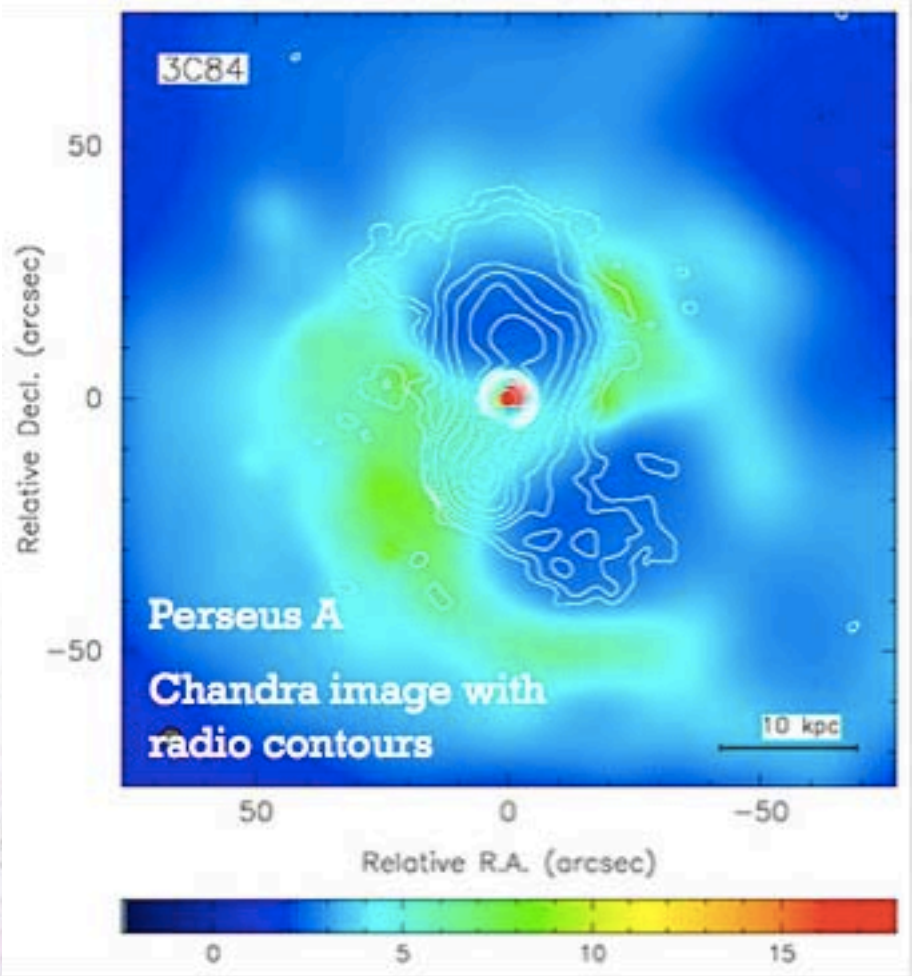

Fabian et al. (2003)

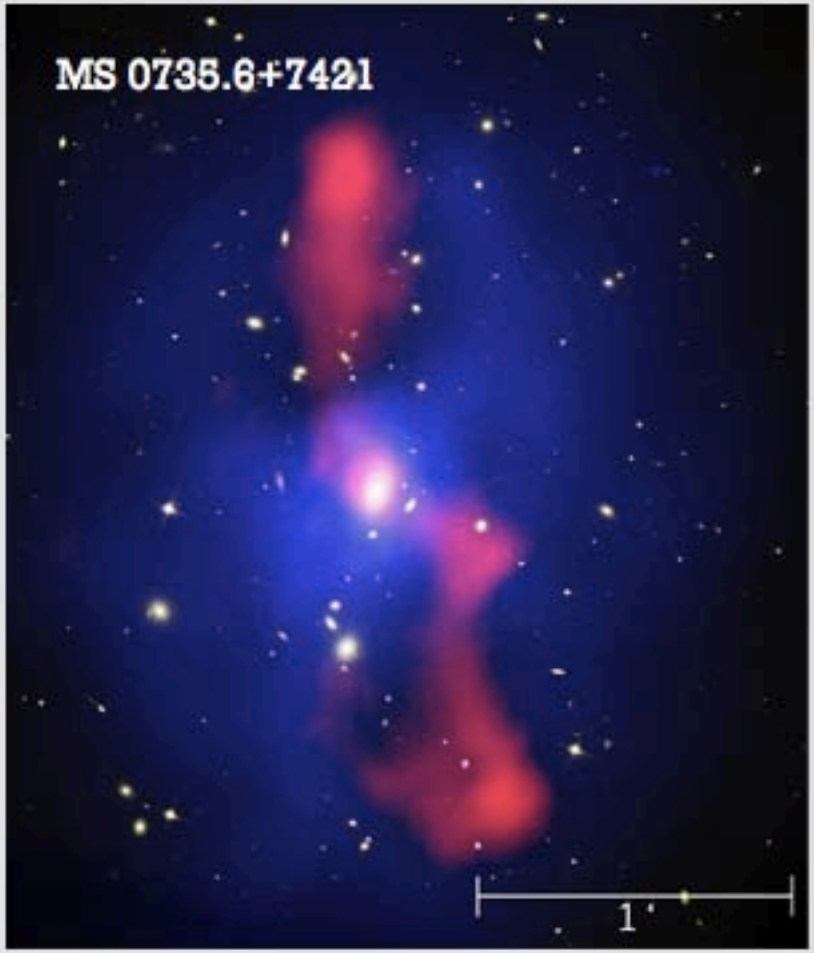

McNamara et al. (2005)

Perseus cluster: Chandra image

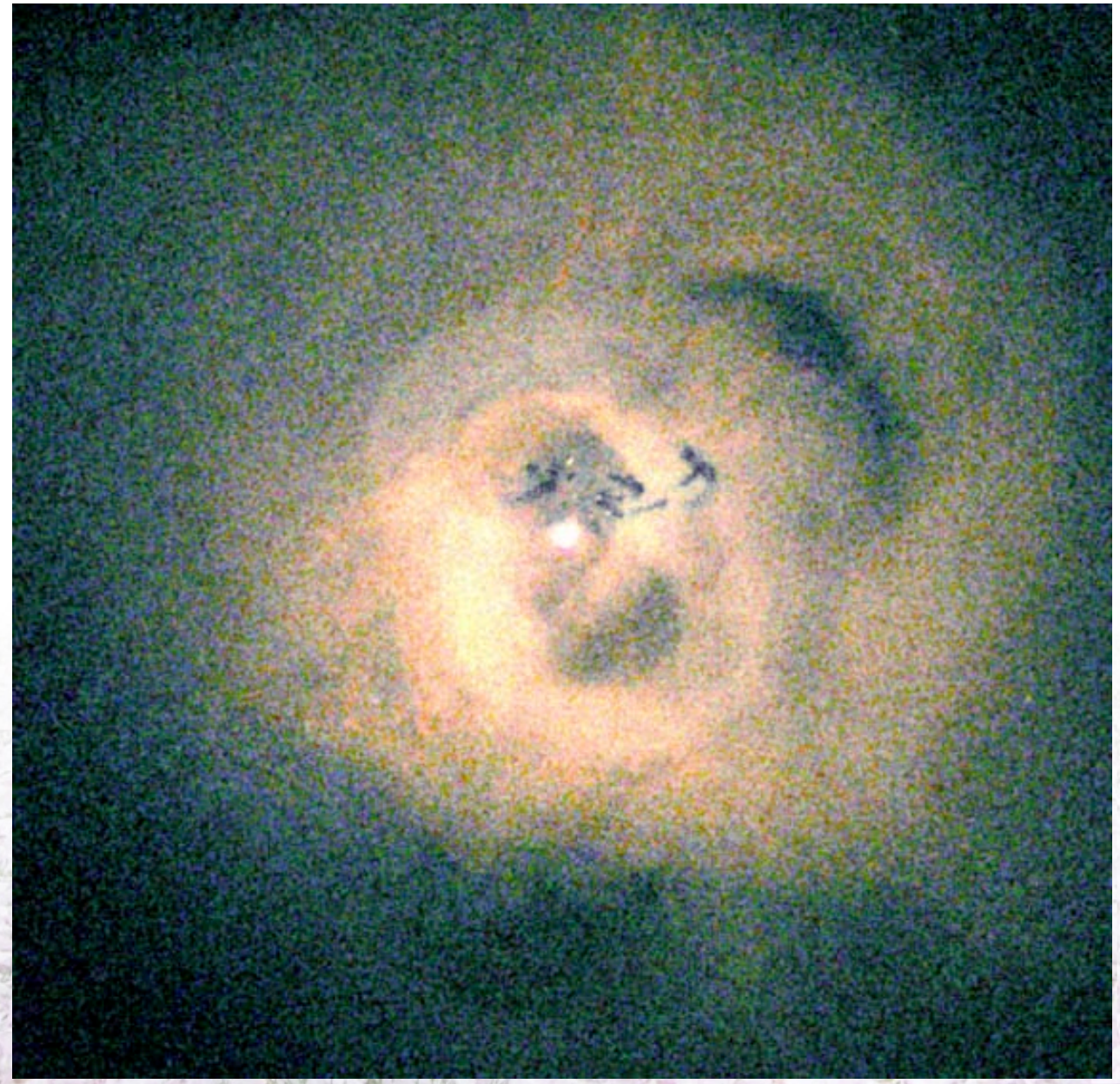

Feedback by jetted AGNs

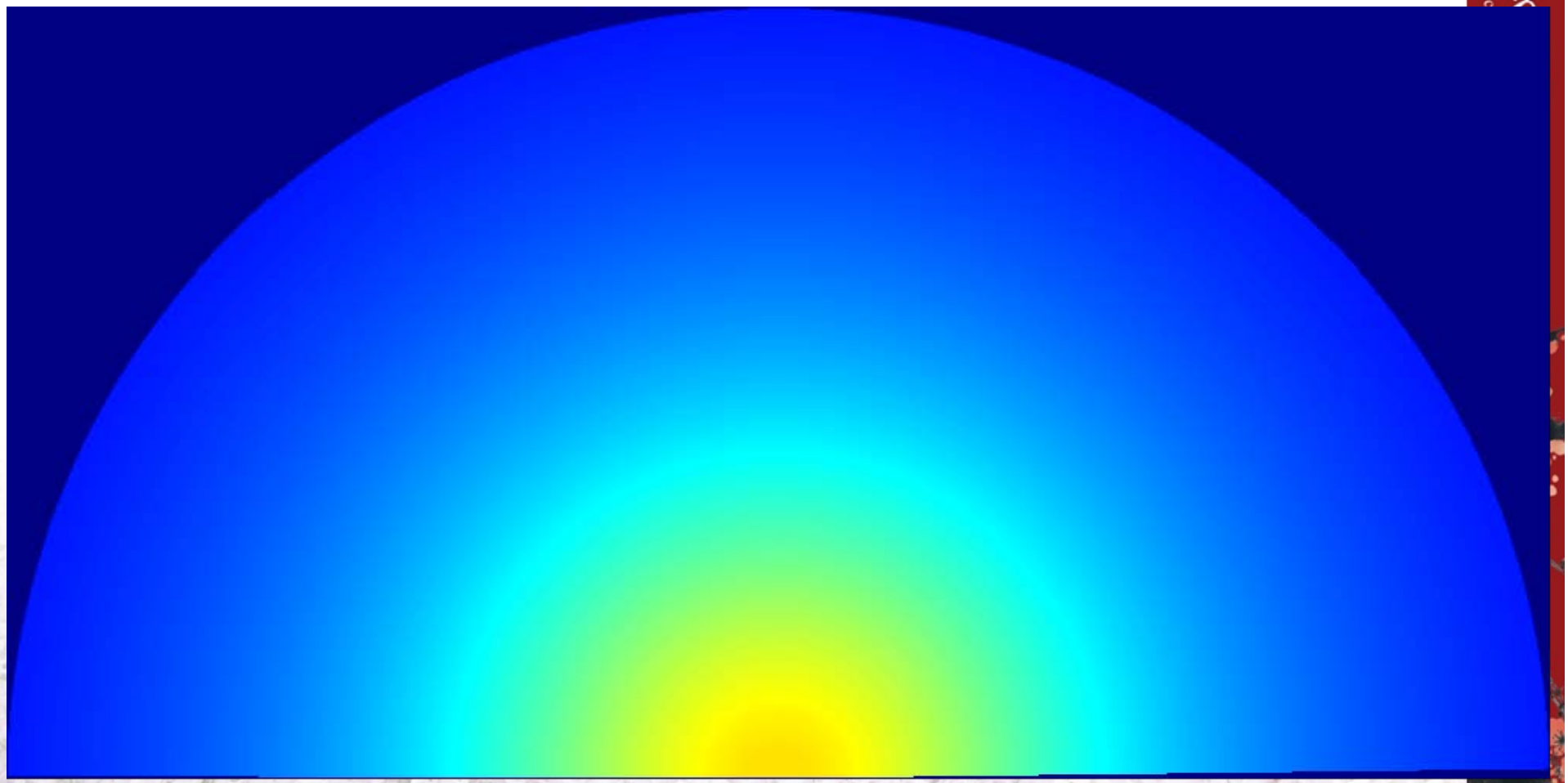

(Vernaleo & Reynolds 2006)

"Theory of everything": multicomponent AGN models

- AGN wind model: multicomponent, multidimension wind not a complete model yet!

  - combine various AGN components (BH, AD, torus, BLR, NLR, HIG, etc.) into a general coherent model, based on observation and speculation

  - such winds likely originate from BH vicinity (perhaps AD surface) and extend all the way to kpc distances, beyond NLR

    * fast disk winds: nearest to BH; lifted from thin AD along B field lines
      - radiation and B pressure provide first kick, then by central radiation field

    * BALs and NALs: most naturally explained by the wind model
      - very high velocity outflows require shielding at their base

    * broad emission lines: made of high-density, optically thick condensations in the wind

    * clumpy torus: natural extension of BLR

    * narrow emission lines: outflow can reach NLR scales and perhaps break into large condensations forming NLR; additional acceleration may be due to radiation pressure force on dust grains

    * HIG outflow: outflowing, highly ionized X-ray gas, with a modest mass outflow rate, is indeed observed in many AGNs

Table 7.1. *AGN components: Location density and ionization parameter*

Component	Distance in r_g	Density	Ionization parameter
Accretion disk	~ 100	$\sim 10^{15}$ cm^{-3}	$U_{\text{oxygen}} = 10^{-3}$–$10^{-1}$
BLR	10^4–10^5	$\sim 10^{10}$ cm^{-3}	$U_{\text{hydrogen}} \sim 10^{-2}$
Torus	10^5–10^6	10^3–10^6 cm^{-3}	$U_{\text{oxygen}} \sim 10^{-2}$
HIG	$\sim 10^6$	10^3–10^5 cm^{-3}	$U_{\text{oxygen}} \sim 10^{-2}$
NLR	10^7–10^8	10^3–10^5 cm^{-3}	$U_{\text{hydrogen}} \sim 10^{-2}$
Starburst	10^7–10^8	10^0–10^3 cm^{-3}	$U_{\text{hydrogen}} = 1$–10^{-2}

To summarize all these possibilities, we show in Table 7.1 a list of all locations considered here with their known (or estimated) densities and the corresponding ionization parameters. The values in the table refer to the illuminated faces of the various components and assume no attenuation between the central source and the location in question. The dimensions are given in gravitational radii, r_g, and the ionization parameters in either U_{oxygen} for X-ray-emitting components or U_{hydrogen} for optical–UV–emitting components. For the conversion between the two, see Table 5.2.

The end